nature protocols

https://doi.org/10.1038/s41596-025-01234-9

Protocol

Check for updates

A universal protocol for ultrafast direct regeneration and upcycling of spent lithium-ion battery cathode materials

Haocheng Ji[1,7], Junxiong Wang[1,2,7], Xiao Qiu[3], Hengyu Ren[4], Haoyu Xue[4], Hao Zhang[1], Guanjun Ji[1,2], Hui-Ming Cheng[5,6] ✉ & Guangmin Zhou[1] ✉

Abstract

The rapid acceleration of global electrification has increased demand for sustainable energy storage, making lithium-ion batteries (LIBs) essential for various applications. However, their limited lifespan presents challenges related to resource waste and environmental risks. Unlike traditional metallurgical methods, which extract key metals from spent cathodes, the direct recycling process repairs damaged materials, maximizing their residual value through effective treatments. Despite widespread interest, systematic protocols to guide interdisciplinary researchers in direct recycling studies remain scarce. Using spent $LiMn_2O_4$ as an example, this protocol outlines a general approach for direct recycling and upcycling of spent LIBs. Initially, the failure condition of the spent cathode is evaluated using X-ray diffraction and inductively coupled plasma analysis to determine appropriate recycling parameters. The resulting recycled products include regenerated $LiMn_2O_4$ and upcycled next-generation cathode materials, such as high-voltage $LiNi_{0.5}Mn_{1.5}O_4$ and Co-free, Li-rich $Li_{1.2}Ni_{0.2}Mn_{0.6}O_2$. Subsequently, electron microscopy, spectroscopic techniques and electrochemical performance tests evaluate recycling effectiveness. This protocol incorporates two representative recycling methods to provide readers with a detailed procedural guide. Solid-phase regeneration forms the basis of most direct recycling technologies; thus, it requires minimal adjustments for broad applicability. Joule heating, a more emerging recycling technology, leverages rapid nonequilibrium reactions, substantially reducing processing time and introducing beneficial structural defects and elemental gradient distributions within the material. Compared to metallurgical methods, solid-phase and Joule heating-based protocols reduce recycling time to ~32 h and 5 h, respectively. Overall, this protocol provides a reliable guide for researchers, promoting sustainable LIB recycling and advancing clean energy research.

A full list of affiliations appears at the end of the paper. ✉e-mail: cheng@imr.ac.cn; guangminzhou@sz.tsinghua.edu.cn

Key points

- This protocol introduces two representative techniques to help readers easily adapt and optimize the methods for implementing a direct recycling process.
- The success of direct recycling hinges on thorough pretreatment and addressing the challenges posed by the failure behavior of spent materials, including lithium replenishment and phase structure recovery.
- The core of direct upcycling lies in constructing a viable direct phase evolution path between the target and initial materials.

Key references

Wang, J. et al. *Nat. Sustain.* **7**, 1283–1293 (2024): https://doi.org/10.1038/s41893-024-01412-9

Wang, J. et al. *Nat. Sustain.* **6**, 797–805 (2023): https://doi.org/10.1038/s41893-023-01094-9

Ma, J. et al. *Nat. Commun.* **15**, 1046 (2024): https://doi.org/10.1038/s41467-024-45091-8

Choi, C. H. et al. *Nat. Chem.* **16**, 1831–1837 (2024): https://doi.org/10.1038/s41557-024-01598-7

Wang, C. et al. *Science* **369**, 521–526 (2020): https://doi.org/10.1126/science.aaz7681

Introduction

With the acceleration of global electrification and intelligent transformation, higher demands are placed on the efficient utilization and storage of renewable clean energy[1,2]. Lithium-ion batteries (LIBs), recognized as one of the best energy storage technologies, have been widely adopted in various sectors of daily life and industry[3,4]. They are used mainly in computers, communication devices, consumer electronics (3C electronic), grid-scale energy storage and electric vehicles, the market for which is expanding rapidly[5,6]. This broad range of applications has fueled a surge in battery demand. It is estimated that by 2030, global battery demand will reach ~2,800 GWh, continuing to rise to over 9,000 GWh by 2050 (ref. 7). However, the lifespan of LIBs is limited, typically between 5 and 8 years, therefore a large number of LIBs will need to be replaced in the near future[8].

However, the long-term storage of spent LIBs presents a potential risk of spontaneous combustion and explosion, and improper handling poses serious safety hazards[9]. Traditional solid waste treatment methods, such as incineration or landfill disposal, inevitably result in environmental pollution, including the release of heavy metals, organic compounds, fluorine and dust. These pollutants can cause long-term environmental damage and pose risks to human health[10,11]. More critically, the supply of key metals such as lithium (Li), cobalt (Co) and copper (Cu), which are essential for manufacturing LIBs, has not kept pace with the rapid growth in battery demand, triggering concerns about a looming supply and demand crisis[12,13]. Therefore, it is crucial to develop efficient and environmentally friendly technologies for recycling spent LIBs[14].

Recycling strategies for spent LIBs

As shown in Fig. 1, the currently developed recycling technologies for spent LIBs can be classified into three progressive categories on the basis of the target product: downcycling, recycling and upcycling[15]. This classification effectively reflects the evolution and advancement of the core concepts underlying spent LIB recycling technology.

Downcycling is a widely used recycling method in industrial production today. It employs mature metallurgical technologies to break down and disrupt the crystal structure of the original

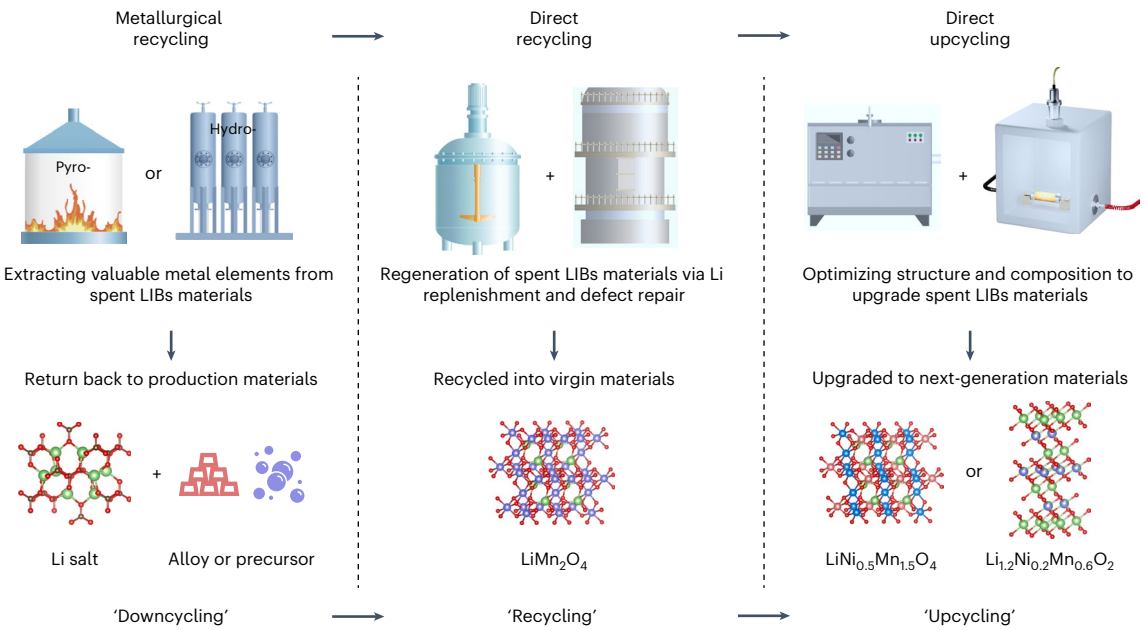

Fig. 1 | A comparison of spent LIB recycling technologies at different stages of development. Metallurgical recycling processes typically downcycle materials, underscoring the need for next-generation recycling technologies that preserve and even upcycle material value.

Table 1 | Comparison of key parameters of spent LIB recycling technologies at different stages of development

Recycling technologies	Cost	Profit	Energy consumption	GHG emissions	Process time	Recycling rate
Metallurgical recycling	●●	●	●●●	●●●	●●●	●●
Direct recycling	●●	●●	●●	●	●●	●●●
Direct upcycling	●●●	●●●	●●	●●	●●	●●●

●Poor, ●●moderate, ●●●excellent. The evaluation is based on the average performance of various recycling technologies, although it may fluctuate depending on the specific characteristics of the recycling method employed. GHG, greenhouse gas.

electrode material through chemical reactions in high-temperature or liquid environments[16,17]. The material is then recombined and undergoes a series of operations before being recrystallized to produce the target product, which is typically an alloy or metal salt with economic value. The essence of this process involves re-refining spent LIB electrode materials into raw materials for production using metallurgical methods. The main techniques include pyrometallurgical and hydrometallurgical recycling. Although these methods are relatively easy to operate and have low equipment and raw material requirements, they come with drawbacks, such as high energy consumption, substantial emissions, lengthy processes and low recycling rates[18]. These processes also consume considerable amounts of energy, generate greenhouse gases and produce industrial wastewater, which contradict the principles of clean technology. These factors limit the ability of the spent LIB recycling industry to capitalize on its potential advantages in terms of high value, low carbon emissions and environmental cleanliness[19,20].

In contrast, direct recycling focuses on repairing the structure of spent LIB electrode materials back to their original state. This process preserves the complete crystal structure of the electrode material, effectively addresses issues such as element loss, structural damage and defects accumulated in the electrode material during prolonged use. By employing simple and efficient treatment methods, direct recycling maximizes the retention of the residual value in spent LIBs[7]. Therefore, this process can also be called the direct regeneration of spent electrode materials. The concept was first proposed by researchers at Argonne National Laboratory in the USA around the turn of the millennium. However, it has only gained attention in the past 5 years, driven by the increasing number of retired LIBs and advancements in LIB technology[7,8,21].

Compared with metallurgical recycling methods, direct recycling is simpler, with higher efficiency. The regeneration of spent electrode materials can be achieved through straightforward separation, pretreatment and lithium replenishment processes. This approach offers clear advantages in terms of profit, energy consumption, efficiency and environmental impact, positioning it as the next generation of battery recycling technology[8] (Supplementary Figs. 1–3 and Supplementary Table 1).

However, the pace of technological progress is accelerating, and the industry's performance benchmarks for LIBs are continuously evolving. In a period of rapid technological iteration, even if spent LIBs are directly regenerated to restore their original performance, they will often lag behind the latest market technical requirements by one to two generations after 5–8 years of service[22]. For instance, in the past decade, the upper cutoff voltage for layered cathode materials such as $LiCoO_2$ has increased from 4.3 V to 4.6 V to fully utilize their theoretical capacity[23]. This new technical benchmark demands higher stability and voltage tolerance, which direct recycling alone may not achieve. Furthermore, as the industry's understanding of materials deepens, emerging materials such as single-crystal Ni-rich cathode materials, $LiFe_xMn_{1-x}O_4$ materials, high-voltage $LiNi_yMn_{2-y}O_4$ spinel oxide cathodes and Li-rich Mn-based cathodes are gaining market attention and are poised to replace older materials in certain applications[24–27]. These shifts have prompted the emergence of a new concept: 'upcycling' spent LIBs. This process goes beyond simple recycling by enhancing the physical properties of the materials or converting them into next-generation materials that meet or exceed the performance benchmarks of contemporary LIBs[28].

Table 1 provides a comprehensive evaluation of three recycling technologies at different stages of development across various dimensions, such as economic performance,

Table 2 | Comparison of key parameters of five direct regeneration methods

Direct regeneration methods	Applicability	Recycling effectiveness	Process efficiency	Environmental impact	Cost	Processing capacity
Solid-phase regeneration	●●	●	●●	●●●	●●●	●●●
Hydrothermal repair	●●	●●	●	●●●	●●	●●
Molten salt-assisted regeneration	●●●	●●●	●	●●●	●●	●●
Solution lithiation regeneration	●●	●●	●	●●●	●●	●●●
Joule heat regeneration	●●	●●	●●●	●●●	●●●	●

●Poor, ●●, moderate, ●●●excellent.

environmental impact and technical efficiency. The assessment is based on the results of a techno-economic analysis of the direct recycling and upcycling cases described in this protocol, with hydrometallurgy serving as the compared technology (Supplementary Figs. 1–3 and Supplementary Table 1).

Our results indicate that direct recycling and upcycling offer higher economic returns, reduced energy consumption and lower greenhouse gas emissions compared with existing techniques. Their shorter, more streamlined processes also cut processing time and boost recovery rates. Consequently, direct recycling and upcycling show substantial potential for widespread adoption to tackle global environmental and energy-related challenges.

Methods for direct regeneration of spent LIB cathode materials

For LIBs, cathode materials are the most expensive components, containing high-value metals such as Li, Co and Ni, making them the most valuable for recycling. As a result, battery recycling efforts focus mainly on the cathode. The synthesis of cathode materials typically involves mixing and sintering specific precursor ratios with lithium salts. In fact, the direct regeneration of cathode materials closely mirrors this synthesis process, essentially using spent cathode materials as raw materials and adding lithium salts to sinter and regenerate the cathodes. Building on this understanding, our research group has transferred knowledge from cathode material synthesis to the direct regeneration of cathodes. This has led to the exploration of various regeneration methods, including solid-phase regeneration[29,30], hydrothermal repair[31,32], molten salt-assisted regeneration[33,34] and solution lithiation[35,36].

However, due to the complex failure mechanisms of spent cathode materials and the varying phase transition paths during both the repair and synthesis processes, the conversion behavior of exogenous Li salts becomes more complicated, and the kinetics of Li^+ replenishment is limited. As a result, direct regeneration through a simple synthesis approach often yields suboptimal results. To address this, our research group has optimized the direct regeneration strategy by focusing on material failure behavior, including surface structure reconstruction and regulation of interface components[37–39].

Moreover, advancements in material synthesis technology have paved the way for innovations in direct regeneration. Recently, researchers have introduced a fast Joule heating synthesis method, which utilizes the heat generated by electric current passing through a conductive material to directly heat raw materials for synthesis. This approach substantially reduces synthesis time while enhancing efficiency and energy utilization[40,41]. This method also introduces controlled defects into the material through a nonequilibrium process, optimizing its performance[42,43]. This ultrafast synthesis technology has now been applied to the recycling of spent cathode materials, demonstrating unique advantages[44,45].

Table 2 compares the key parameters of the five direct regeneration methods, including their applicability, recycling effectiveness, process efficiency, environmental impact, cost and processing capacity. Overall, the direct regeneration process of cathode materials generally involves two key steps: Li compensation and structural rearrangement. Typically, structural rearrangement occurs through thermodynamic processes at high temperatures, making heat treatment unavoidable in most cases. Thus, all direct regeneration processes can be considered as process adjustments based on solid-phase regeneration methods. In this protocol, we will focus on the basic solid-phase regeneration method and the novel Joule heat ultrafast

regeneration method as representative techniques to illustrate the overall process of direct recycling for spent LIBs cathode materials.

Upcycling pathways of spent LIBs cathode materials

The main upcycling pathways for spent cathode materials can be categorized into two types. The first involves cases in which the structure and composition of the spent materials are largely similar to the target product, requiring only improvements in physical properties, characteristics or performance indicators. In such cases, direct upcycling can be readily achieved. Essentially, this process combines direct regeneration with modification methods, provided the failure characteristics of the spent materials are thoroughly analyzed and their defects accurately utilized. Our group has demonstrated that the intrinsic structural defects in spent $LiCoO_2$ can effectively lower the migration energy barrier of exogenous doping elements, enhancing their atomic diffusion and enabling precise vacancy occupation. By integrating Mg and Al co-doping into the solid-phase regeneration process, we successfully upcycled spent $LiCoO_2$ into high-voltage $LiCoO_2$ in a single step, achieving ultrastable cycling at 4.6 V (ref. 28). Similarly, we applied this approach to spent Ni-rich cathode materials, replacing the recycling method with molten salt-assisted regeneration. This method not only enables high-voltage upgrading but also leverages the eutectic molten salt's control over crystal growth to simultaneously achieve single-crystal upgrading, aligning with market trends and delivering dual benefits[46].

In another scenario, the spent material differs from the target product not only in characteristics and performance indicators but also in structure or composition. The conventional approach in such cases is to first downcycle and recycle the material, converting its elements into the corresponding precursor compounds, and then upcycle it into the next-generation cathode material through resynthesis. For instance, our group proposed using reusable, green deep eutectic solvents to convert spent $LiFePO_4$ and $LiMn_2O_4$ cathodes into solid solution precursors, which were then upcycled into high-voltage polyanion materials $LiFe_{0.5}Mn_{0.5}PO_4$ (ref. 47). This approach effectively enhanced the average voltage and energy density of the material. Additionally, we reported a subtractive recycling strategy, which involves selectively extracting equal amounts of Co and Ni from degraded $LiNi_{0.5}Co_{0.2}Mn_{0.3}O_2$ and $LiMn_2O_4$ mixed cathodes. The remaining transition metals were then converted into hydrochloride precursors with the corresponding elemental ratios and further upcycled into 5 V-grade spinel $LiNi_{0.5}Mn_{1.5}O_4$ cathode materials[48]. To achieve one-step direct upcycling in such cases, it is crucial to maintain a continuous phase transition connection between the spent material and the target product, as well as to design and adopt suitable methods in advance. This protocol will use two direct upcycling examples to illustrate the design concepts and experimental procedures.

Applications of the protocol

The main applications of this technique are direct recycling and upcycling of spent LIB electrode materials. This technique bridges the gap between waste management and material performance enhancement, providing practical engineering solutions that align with United Nations Sustainable Development Goals 7 and 12. The direct recycling and upcycling technology for spent LIBs is an interdisciplinary field that integrates materials science, environmental science, chemistry and engineering. Breakthroughs in this area require contributions from experts with diverse backgrounds. However, since this research is closely tied to engineering science, many technical details—such as pretreatment operations and reagent dosages—depend heavily on practical experience. To address this, this protocol aims to provide technical guidance for interdisciplinary researchers new to the field, helping to minimize the waste of manpower and resources during familiarization and experimental exploration. The solid-phase regeneration method detailed in this protocol serves as the foundation for most emerging direct recycling technologies. Readers are encouraged to expand and optimize the experimental procedures on the basis of the specific characteristics of this method. Furthermore, due to the similarities between the recycling and synthesis processes, the operations and insights presented in this protocol can also be applied to the synthesis of secondary ion battery cathode materials.

Limitations of the protocol

Although the direct regeneration strategy described in this protocol can be applied to most spent cathode materials, certain limitations remain.

First, the current technology heavily relies on accurate analysis and judgment of the failure state of spent materials. Moreover, there is no universal direct recycling strategy applicable to cathode materials of different types, failure behaviors and failure degrees. A suitable recycling method must be selected on the basis of the specific material state. However, as noted earlier, the experimental procedures of most direct recycling strategies can be expanded based on this protocol.

Second, as an industry-oriented research topic, direct regeneration technology for spent LIBs ultimately needs to be scaled for production applications at the tonnage level or beyond. Experience from scaling up laboratory processes from the gram to the kilogram level indicates that larger-scale production requires adjustments to process parameters on the basis of production conditions.

Third, no direct regeneration strategy currently exists that is broadly effective for complex mixed cathodes. We will continue to focus on developing a general direct regeneration strategy suitable for large-scale applications.

As an emerging technology, Joule heating still faces notable limitations in the direct regeneration of spent LIB materials.

One major challenge is large-scale implementation. Although Joule heating has demonstrated industrial-level productivity for graphene, research on synthesizing inorganic materials with this method remains limited to gram-scale experiments. This gap makes it difficult to apply Joule heating to large-scale direct regeneration and upgrading of spent LIB electrodes. Therefore, equipment optimization is needed to ensure uniform temperature and current distribution when processing larger samples, thereby safeguarding the safety, consistency and uniformity of the recycling process.

Moreover, optimizing Joule heating conditions presents another hurdle. The relevant parameters—such as heating temperature, heating/cooling rates and the number of pulses—can be adjusted across a wide range. However, because each material system and recycling goal demands different optimal conditions, identifying the most effective parameter set may extend development times.

Additionally, as mentioned earlier, the direct upcycling strategy described in this protocol requires a case-by-case evaluation before designing a plan. This involves analyzing the feasibility of the phase transition path between the initial material and the target product, followed by a targeted design tailored to the direct regeneration process.

Overview of the procedure

The procedure is divided into five main parts:

- Spent battery disassembly and pretreatment
- Failure analysis of spent cathode materials
- Direct regeneration and upcycling of spent cathode materials
- Regenerated cathode material characterization
- Electrochemical performance verification

The overall experimental design of this protocol is illustrated in Fig. 2. We selected $LiMn_2O_4$ as the representative material for two key reasons. First, most research papers often overlook the development of direct regeneration strategies for this material. Second, as Mn-based materials are poised to become mainstream in next-generation cathode materials[49,50], starting with spent $LiMn_2O_4$ provides a strong foundation for designing effective direct upcycling pathways.

Spent battery disassembly and pretreatment

We began by obtaining a spent pouch cell with $LiMn_2O_4$ as the cathode material from a manufacturer that we are collaborating with. After fully discharging the cell by soaking it in salt water, it was manually disassembled in the laboratory to isolate its components. The cathode electrode was cleaned with dimethyl carbonate (DMC) to remove residual electrolyte and side

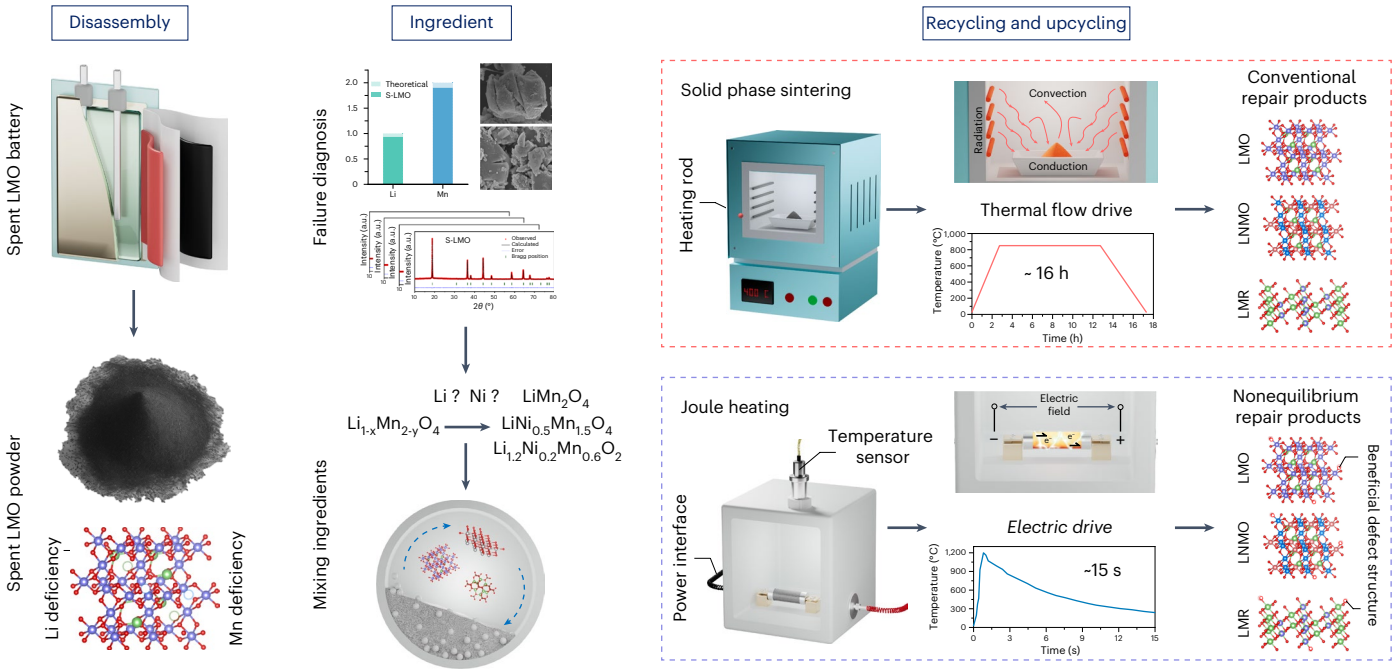

Fig. 2 | The overall experimental design of this protocol. The main experimental process includes the following: (1) disassembling spent LIBs to collect and pre-treat the spent cathode materials; (2) calculating the required additives on the basis of failure analysis results and the target product composition; and (3) selecting an appropriate method for direct recycling or upcycling.

reaction products, and the cathode material powder was physically separated from the Al foil current collector. The powder was then ground, sieved to remove large particles and impurities, and washed with 1-methyl-2-pyrrolidinone (NMP) and NaOH aqueous solutions to eliminate the binder, side reaction products and Al debris. Finally, the material was dried to obtain the spent cathode powder for recycling.

Failure analysis of spent cathode materials

To optimize the regeneration process and minimize material waste, failure analysis was performed on the powders using inductively coupled plasma–optical emission spectrometry (ICP–OES) and X-ray diffractometry (XRD) tests to assess lithium loss and phase structure degradation. On the basis of these results, a tailored direct regeneration and upcycling scheme was designed. The spent material powder was mixed with a lithium source and a nickel source via ball milling, following a carefully specified batching standard for exogenous lithium salts—a critical factor for experimental success.

Direct regeneration and upcycling of spent cathode materials

The spent materials were then directly recycled using solid-phase regeneration and Joule heat-assisted regeneration methods, employing a muffle furnace and Joule heat device, respectively. For the solid-phase method, additional water washing and re-sintering steps were included to ensure complete recycling. Using the Joule heat method, we also demonstrated one-step direct upcycling of spent $LiMn_2O_4$. The two classic cathode materials, $LiNi_{0.5}Mn_{1.5}O_4$ and $Li_{1.2}Ni_{0.2}Mn_{0.6}O_2$, which show potential for future market applications, are used here as examples to demonstrate the versatility of this method. Researchers can adapt this process to produce manganese-based materials with other components, depending on specific experimental needs. This includes layered Li-rich materials with the classic composition of $Li_{1.2}Ni_{0.13}Co_{0.13}Mn_{0.54}O_2$, rock salt-phase Mn-based Li-rich materials and others. Additionally, the method can be combined with conventional modification techniques, such as element doping and surface engineering, to further optimize material performance.

Regenerated cathode material characterization

The regenerated cathode materials were characterized using multiple techniques: ICP–OES to confirm elemental replenishment, XRD to assess phase evolution, scanning electron microscopy (SEM) to analyze microscopic morphology, transmission electron microscopy (TEM) to study local lattice phase structures and electron paramagnetic resonance (EPR) to evaluate the impact of the nonequilibrium phase repair process on material defect behavior.

Electrochemical performance verification

Finally, to evaluate the regeneration and upcycling performance, the recycled material powder was mixed with NMP and polyvinylidene difluoride (PVDF), coated onto Al foil to fabricate electrodes and assembled into half-cells with Li metal as the counter electrode. Long-cycle and rate performance tests were conducted, and the results were compared with those of the spent materials and commercial materials.

Key steps of the protocol

Based on experimental experience, the key steps affecting the direct regeneration process for interdisciplinary researchers new to this field are as follows:

1. Thoroughly discharge the spent batteries (Step 3).
2. Effectively clean the collected cathode material powder to completely remove impurities (Steps 11–17).
3. Accurately determine the lithium replenishment amount on the basis of failure analysis and the lithium replenishment mechanism (Steps 40, 42).
4. Optimize the heat treatment process by setting the environment, temperature, duration, and procedure according to the material's condition (Steps 51, 67, 73, 76).
5. Water washing and re-sintering steps (Steps 52–56).

Special reminder

Before adopting the processes described in research papers claiming to achieve direct recycling of spent cathode materials, carefully examine the charge and discharge curves of the spent cathode materials presented in the literature. In some cases, if the charge-specific capacity is extremely low but the discharge-specific capacity is high or even close to the standard specific capacity, the material being treated may not be an actual spent cathode material. Instead, it could be a lithium-deficient cathode material created through electrochemical or chemical delithiation. As a result, the regeneration methods described in these studies may not be fully applicable to the treatment of actual spent cathode materials.

Materials

Reagents

▲ **CAUTION** Some reagents used in this protocol are volatile solvents or strong acids that can corrode the skin or damage the respiratory system. The experiment must be conducted in a qualified chemical laboratory equipped with essential safety facilities, including eyewashes and fire-fighting equipment. Operators must wear appropriate personal protective equipment, such as laboratory coats, explosion-proof goggles and nitrile gloves. The preparation of precursor solutions should be carried out in a ventilated fume hood and clearly marked with caution labels. All chemicals must be stored in appropriate cabinets or explosion-proof refrigerators. Before use, refer to the Material Safety Data Sheet (www.msds.gs) for proper handling and storage instructions.

- Spent lithium manganate pouch cell ($LiMn_2O_4$, Ronbay)
  ▲ **CAUTION** Spent lithium-ion pouch cells pose a fire hazard. When heated, ruptured or exhibiting abnormal phenomena such as bloating, they can burn or explode. Store them in explosion-proof boxes whenever possible.

- Sodium chloride (NaCl, 99.5%, Macklin, cat. no. S805275)
- DMC (98%, Macklin, cat. no. D807386)
  ▲ **CAUTION** DMC is a slightly toxic organic solvent. Always wear appropriate protective equipment when handling it, avoid contact with skin and eyes and prevent inhalation of vapors and fumes. Keep it away from heat sources and use it in a well-ventilated fume hood.
- NMP (>99.5%, Macklin, cat. no. M813015)
  ▲ **CAUTION** NMP is a slightly toxic organic solvent. Always wear appropriate protective equipment when handling it, avoid contact with skin and eyes and prevent inhalation of vapors and fumes. Keep it away from heat sources and use it in a well-ventilated fume hood.
- Phytic acid (50%, Macklin, cat. no. P816021)
  ▲ **CAUTION** Phytic acid is strongly acidic. Always wear appropriate protective equipment when handling it, avoid contact with skin and eyes. Store it in a cool and dry place.
- Anhydrous ethanol (99.7%, Macklin, cat. no. E809061)
  ▲ **CAUTION** Anhydrous ethanol is highly volatile and extremely flammable. Keep it away from heat sources during both use and storage.
- Sodium hydroxide (NaOH, 95%, Macklin, cat. no. S835850)
  ▲ **CAUTION** NaOH is a strong alkali with serious irritant and corrosive properties. Its dust or fumes can irritate the eyes and respiratory tract, while direct contact with skin or eyes can cause burns. Always wear protective gloves and goggles during handling and avoid direct contact.
- Concentrated hydrochloric acid (HCl, 37%, Aladdin, cat. no. H399657)
  ▲ **CAUTION** Concentrated HCl is a highly corrosive and volatile strong acid with strong irritant properties. Its fumes can severely irritate the eyes and respiratory tract, while direct contact with skin or eyes can cause irreversible damage. Always wear protective gloves and goggles when handling materials. Avoid direct contact with substances and ensure that the process is conducted in a well-ventilated fume hood.
- Concentrated nitric acid (HNO_3, 65–67%, Sigma-Aldrich, cat. no. 84378)
  ▲ **CAUTION** Concentrated HNO_3 is a highly corrosive and volatile strong acid with strong irritant properties. Its fumes can severely irritate the eyes and respiratory tract, while direct contact with skin or eyes can cause irreversible damage. Always wear protective gloves and goggles when handling materials. Avoid direct contact with substances and ensure that the process is conducted in a well-ventilated fume hood.
- Lithium carbonate (Li_2CO_3, 99.5%, Macklin, cat. no. L812282)
  ▲ **CAUTION** Store in ventilated dry place, pay attention to prevent rain and water.
- Lithium hydroxide (LiOH, 98%, Macklin, cat. no. L812391)
  ▲ **CAUTION** Strong corrosion. Do not breathe dust. Wear suitable protective clothing, gloves and eye/face protection when handling it. Store it in a dry and clean warehouse. Keep it away from fire and heat sources. Keep it the package sealed.
- Lithium acetate (CH_3COOLi, 99.99%, Aladdin, cat. no. L118858)
- Nickel oxide (NiO, 99%, Aladdin, cat. no. N108314)
  ▲ **CAUTION** May cause sensitization by skin contact. May cause cancer by inhalation. Wear suitable protective clothing and gloves when handling it. Store it in a dry and clean warehouse. Keep it away from fire and heat sources.
- Graphite paper (0.05 mm, Hebei King Carbon Tech)
- PVDF (Canrd, cat. no. MA-EN-BI-0023)
  ▲ **CAUTION** PVDF is prone to decomposition when exposed to water. Keep it away from moisture and store it in a dryer or glove box.
- Acetylene black (99.9%, Canrd, cat. no. MA-EN-CO-040161)
- Aluminum foil (99.999%, Cailiaoren, cat. no. KY05748)
- Lithium ion battery electrolyte (1 M $LiPF_6$ solution in EC:DMC:DEC of 1:1:1 vol%, DoDoChem, cat. no. 21324-40-3)
  ▲ **CAUTION** Electrolyte is a slightly toxic solvent. Always wear appropriate protective equipment when handling it, avoid contact with skin and eyes. Store it in glove box.
- Polypropylene diaphragm (Celgard, 2500)

- Li metal chip (Li, China Aviation Lithium Battery)
  ▲ **CAUTION** Li metal is highly reactive and corrosive, capable of causing irritation or burns to the eyes and skin. It oxidizes and deteriorates quickly when exposed to air, releasing hydrogen and potentially producing sparks when reacting with water. Store and handle it in an inert environment, such as a glove box, to ensure safety.
- Commercial $LiMn_2O_4$ cathode powder (Canrd, cat. no. MA-EN-CA-001601)
  ▲ **CAUTION** Keep it away from moisture and store it in a dryer or glove box.
- Commercial $Li_{1.2}Ni_{0.2}Mn_{0.6}O_2$ cathode powder (Canrd, cat. no. MA-EN-CA-0043)
  ▲ **CAUTION** Keep it away from moisture and store it in a dryer or glove box.
- Commercial $LiNi_{0.5}Mn_{1.5}O_4$ cathode powder (Canrd, cat. no. MA-EN-CA-000103)
  ▲ **CAUTION** Keep it away from moisture and store it in a dryer or glove box.

Equipment

- Deionized pure water machine (Ulupure, model no. UPH-11-10TNP)
- Vibration dehydrator (Dongguan Bochang Environmental Protection Technology, model no. BC-1)
- Digital multimeter (Victor, model no. VC890C)
- Muffle furnace (Shenzhen Kejing Star Tech., model no. KSL-1100X-S)
  ▲ **CAUTION** Heating equipment, ensure the furnace temperature has stabilized at a safe level before opening the door during use and ensure the environment is ventilated to avoid affect the sintering process. Always wear heat-insulating gloves when handling samples to prevent burns.
- Constant temperature blast oven (Shanghai Jinghong, model no. DHG-9031A)
  ▲ **CAUTION** Heating equipment, ensure the furnace temperature has stabilized at a safe level before opening the door during use. Always wear heat-insulating gloves when handling samples to prevent burns.
- Vacuum blast oven (Shanghai Yiheng Scientific Instrument, model no. DZF-6050)
  ▲ **CAUTION** Heating equipment, ensure the furnace temperature has stabilized at a safe level before opening the door during use. Always wear heat-insulating gloves when handling samples to prevent burns.
- Filtration device (Delvstlab, model no. 250ml)
- Magnetic stirrer (Hunan Lichen Instrument, model no. H55-pro)
- Fume hood (Covok, model no. 1800 mm*800 mm*2350 mm)
- Glove box (Shanghai Mikrouna Mech. Tech., model no. Super series)
  ▲ **CAUTION** Inert gas protection equipment. Water content less than 0.01 ppm, oxygen content less than 0.01 ppm. During the operation, care should be taken to protect the working gloves from being damaged.
- Drying cabinet (Shanghai Yiheng Scientific Instrument, model no. BPG-9070A)
- Inductively Coupled Plasma–Optical Emission Spectrometer (Arcos, model no. 2-MV)
- X-ray diffractometer (Rigaku, model no. MiniFlex600)
  ▲ **CAUTION** X-ray radiation equipment, do not open the protective cover door during the experiment. Take precautions to avoid direct exposure to X-rays and, if possible, wear protective equipment to minimize radiation exposure.
- Microwave digester (Shanghai Sineo, model no. Tank)
  ▲ **CAUTION** Heating equipment, ensure the cavity temperature has stabilized at a safe level before opening the door during use. Always wear heat-insulating gloves when handling samples to prevent burns.
- Planetary ball mill (Mitr, model no. YXQM-1L)
  ▲ **CAUTION** Rotary grinding equipment. Ensure that the device has come to a complete stop and has reached a safe level before opening the door during use.
- Joule heat equipment (Shenzhen Zhongke Jingyan Technology, model no. HTS)
  ▲ **CAUTION** Heating equipment, ensure the furnace temperature has stabilized at a safe level and the energized circuit is disconnected before opening the door during use. Always wear heat-insulating gloves when handling samples to prevent burns.
- Field-emission scanning electron microscope (ZEISS, model no. SUPRA-55)

- Field-emission transmission electron microscope (JEOL, model no. JEOL-3200FS)
- TEM sample holder (JEOL, model no. EM-31640)
- EPR (CIQET, model no. EPR200M)
- X-ray photoelectron spectroscopy (XPS) (Thermo Fisher, model no. ESCA LAB 220I-XL)
- Analytical balance (Sartorius, model no. BSA224S-CW, 0.1 mg resolution)
- Analytical balance (Sartorius, model no. QUINTIX65-1CN, 0.01 mg resolution)
- Slurry defoaming machine (Sienox, model no. SIE-MIX90)
- Automatic thick film coater (Shenzhen Kejing Star Tech., model no. MSK-AFA-H200A)
  ▲ **CAUTION** Operate it inside a fume hood to facilitate the extraction and adsorption of a large amount of volatile organic solvents. Always wear appropriate protective equipment when handling it, avoid contact with skin and eyes, and prevent inhalation of vapors and fumes.
- Precision disc cutting machine (Shenzhen Kejing Star Tech., model no. MSK-T10)
- Battery sealing machine (Shenzhen Kejing Star Tech., model no. MSK-110)
- Battery test system (NEWARE, model no. CT-4008T-5V)
- 500 mesh sieve (Lvruo, model no. 52152)
- Pipette (DLAB Scientific, model no. YEA2BAH0062949)
- 200 mesh copper mesh (Canrd, model no. MA-EN-CU-0018)
- Single side polished Si/SiO_2 wafer (Cailiaoren, cat. no. KY01004)

Software

EverBatt2023 (https://www.anl.gov/amd/everbatt)
OriginPro (https://www.originlab.com)
MDI Jade (https://www.icdd.com/mdi-jade)
FullProf (https://www.ill.eu/sites/fullprof/php/downloads.html)
Digital Micrograp (https://www.gatan.com/products/tem-analysis/gatan-microscopy-suite-software)
NEWARE BTS9.0 (https://www.neware.com.cn/)

Reagent setup

Deionized water

In this protocol, the deionized water was self-produced by the laboratory Ulupure de-ion pure water system (tap water source), with a resistivity of 13–17.5 MΩ/cm at 25 °C and heavy metal ion <0.1 ppb.

Others

The setup process for other reagents involved in this protocol is detailed in the 'Procedure' section.

Equipment setup

Glass/plastic equipment

All glass or plastic utensils used in this protocol must be thoroughly cleaned with detergent before use. Rinse them sequentially with tap water, deionized water and anhydrous ethanol. Then, dry the utensils in blast oven at 60 °C and use a ear bulb to remove any remaining sticky impurities.

Others

The setup process for other reagents involved in this protocol is detailed in the 'Procedure' section.

Software setup

Techno-economic analysis setup

In this protocol, we conduct a techno-economic analysis of various recycling technology routes using a standardized benchmark of one ton of spent $LiMn_2O_4$//graphite pouch batteries. Costs are categorized into raw materials, reagents, labor, energy and water, equipment depreciation, pretreatment and environmental protection. As production process costs—including

equipment depreciation, labor and other factors—are difficult to estimate directly, we use data from the EverBatt 2023 database (provided by Argonne National Laboratory) to derive specific values. To calculate potential benefits, we assume that all recovered components have some value that offsets recycling costs. However, since the actual value of separators, electrolytes and shells is difficult to determine, these items are excluded from our benefit analysis. Detailed process-based cost and revenue models are provided in the original data for the techno-economic analysis (Supplementary Table 1). The total life-cycle energy consumption and greenhouse gas emissions for the three recycling processes encompass material use, energy and process emissions, and are also evaluated using the EverBatt model.

FullProf refinement setup

In this protocol, XRD patterns of the powdered sample were refined using the FullProf program. The specific refinement sequence is as follows:

1. Zero point and scale
2. Cell parameters of the material
3. Peak shape parameters
4. Background of the XRD data
5. Preferred orientation of the crystal
6. Shape factor
7. Atomic coordinates
8. Symmetry parameters
9. Atomic occupancy
10. Atomic displacement parameters for each atom

During the refinement steps 1–9, new parameters are added sequentially in the specified order for synchronous refinement. Once the atomic occupancy refinement converges, that parameter is deselected and each atom's displacement parameters are refined independently. If a parameter substantially deviates from its expected value, it is necessary to adjust the refinement sequence and flexibly modify the preset values. Throughout the refinement process, all parameters are constrained within ranges of physical relevance, and the final confidence factor is ensured to remain within a reasonable range.

Procedure

Spent battery disassembly and pretreatment

● **TIMING 45 h**

▲ **CRITICAL** There are two main methods for obtaining spent LIB electrode materials[29,51]. One involves manually disassembling the batteries to obtain spent cathode/anode material powder (Steps 1–8). The other involves sourcing black mass directly from battery disassembly manufacturers, who produce it by crushing and sorting waste batteries. In this protocol, the treatment of such black mass begins at the pretreatment stage (Step 9).

1. Evaluate the basic information and condition of spent LIBs, including battery type, state of health and state of charge. This evaluation relies mainly on information from sources such as the battery nameplate, battery passport and basic electrochemical testing. For batteries lacking essential information, simple pulse testing combined with machine learning based on feature engineering can provide an accurate evaluation[52,53].
2. Prepare an aqueous NaCl solution and adjust the brine concentration to 10–15% (wt/vol%) by controlling the amount of NaCl added.
3. Transfer the spent LIBs into the prepared NaCl solution for chemical discharge, the solution should be added in a volume sufficient to fully submerge the spent LIBs. Adjust the soaking time on the basis of the battery type, and remove the batteries when their voltage drops below 1.5 V (Supplementary Fig. 4).

   ▲ **CAUTION** The saltwater discharge process utilizes the battery's positive and negative electrodes as the cathode and anode, respectively, to consume the residual power through

electrolysis in the solution. This process may generate harmful exhaust gases, so it is essential to implement protective measures and conduct the operation in professional equipment, such as fume hoods. Additionally, the wastewater generated after the reaction may contain leaked electrolytes, fluorides, acidic byproducts and potentially harmful heavy metal ions such as nickel, cobalt, manganese, copper and aluminum, as well as various organic pollutants. Owing to its toxicity and environmental risks, direct discharge of such wastewater is prohibited under environmental regulations. Therefore, it must be collected in designated chemical waste containers and handed over to certified hazardous waste disposal companies. The treatment process typically involves acid–base neutralization, heavy metal precipitation, organic pollutant removal, desalination, and further purification to meet discharge standards.

▲ **CRITICAL STEP** The discharge process must be fully completed. If necessary, a combination of physical and chemical discharge should be employed to ensure complete discharge of the spent battery. Physical discharge refers to the process of discharging a battery by connecting it to an external resistive load, allowing the remaining energy to be safely dissipated in the form of heat. Incomplete battery discharge impacts both safety and regeneration accuracy. From a safety perspective, partially discharged batteries retain more lithium on the anode electrode, increasing the risk of internal chemical reactions or short circuits during disassembly, which may lead to explosions or fires. From a recycling process standpoint, the cathode electrode in such batteries remains lithium deficient, potentially leading to misjudgment of material degradation and increased consumption of reagents during subsequent direct regeneration.

4. After discharge, transfer the spent LIBs to a vibration dehydrator to remove surface moisture, reducing it to less than 5%.

   ▲ **CAUTION** Before operating the vibration dehydrator, ensure that the safety door is properly closed. During use, carefully monitor the equipment's overall vibration amplitude. Excessive vibration can damage the equipment, lead to machine failure and even pose a risk to personal safety.

5. Select the appropriate tools to remove the aluminum plastic film or steel shell on the basis of the battery type. The main commercial types of LIBs include pouch cells, cylindrical cells and prismatic cells. Pouch cells typically have soft shells made of aluminum–plastic composite film, which can be easily removed with scissors. In contrast, cylindrical and prismatic cells have rigid shells made of nickel-plated steel and aluminum alloy, respectively, and usually require cutting tools for disassembly.

   ▲ **CAUTION** Take safety precautions to prevent cuts from sharp blades.

6. Separate the components inside the battery cell, including the Al foil current collector coated with cathode material, the Cu foil current collector coated with anode material and the diaphragm (Supplementary Fig. 5).

   ▲ **CAUTION** This step requires personal safety protection and should be carried out in a glove box whenever possible. If operating in a glove box is not feasible, ensure that gloves and masks are worn and the environment is well ventilated, as the electrolyte is highly volatile and potentially harmful. Additionally, take fire prevention precautions. After disassembly, close attention should be paused to the color of the negative electrode. If the graphite anode appears dark yellow or golden yellow, it indicates a high residual lithium content, which is highly reactive and may ignite upon contact with water or other reagents.

7. Soak the electrode coated with active material in DMC solvent to remove residual electrolyte and side reaction products. Take it out after standing for 20 min, wipe it and dry it.

   ■ **PAUSE POINT** Long-term storage in a normal atmospheric environment can lead to further embrittlement and phase changes of the electrodes and active materials, making recycling more challenging. It is recommended to transfer them to a dry room or glove box as soon as possible.

8. Strip the active material of spent $LiMn_2O_4$ cathode powder from the current collector. Three methods can be chosen on the basis of the electrode characteristics. In most cases, mechanical

separation is broadly applicable, but the process is relatively labor intensive and unsuitable for large-scale applications. Heat treatment separation requires careful consideration of the cathode material's thermal stability to avoid degradation. Solution-based separation is more appropriate for electrodes using water-based binders. For electrodes with organic binders, a suitable solvent system must be selected on the basis of the literature.

- Mechanical separation: use a knife, spoon, or other hard objects to separate the active material powder from the current collector
- Heat treatment separation: transfer the electrode to a muffle furnace and heat it to 400 °C for 20 min to inactivate the binder and separate the active material from the current collector
- Solution treatment separation: prepare a solution using phytic acid or other substances, and soak the electrode for 5 min to inactivate the binder and separate the active material[54]. If the binder is water based, separation can be achieved by water immersion combined with ultrasonic treatment

◆ **TROUBLESHOOTING**

9. Transfer the collected spent $LiMn_2O_4$ cathode powder to an agate mortar and grind it to separate the agglomerated and flaked particles.
10. Sieve the ground powder through a 500 mesh sieve to remove large impurities and agglomerates.
11. Transfer the spent cathode powder to an NMP reagent for cleaning, with a solid:liquid ratio of ~1:20. Stir the mixture for 3 h at 500 rpm.
    ▲ **CAUTION** NMP is volatile and irritating. During operation, avoid contact with skin and eyes, inhalation and exposure to fire.
    ▲ **CRITICAL STEP** The cleaning process directly affects the performance of the subsequent direct regeneration of materials. Residual fluorine-containing organic impurities may diffuse into the bulk phase and react on the surface during the subsequent heating repair process, disrupting the original balance between the repair reaction and thermal decomposition. This step is especially critical when treating black mass raw materials.
12. Separate the material by suction filtration and then wash three times with ethanol. Each wash follows a standard procedure: ethanol is gently poured along a glass rod onto the sediment on the filter paper until it is fully submerged. After allowing it to stand for 1 min, a vacuum pump is activated to draw the liquid through the filter.
13. Transfer the treated cathode powder to a blast oven at 100 °C and leave it there until it is completely dry.
14. Prepare an aqueous NaOH solution and adjust the concentration to 1 mol/L by controlling the amount of NaOH added.
    ▲ **CAUTION** NaOH is highly irritating and corrosive; therefore, safety precautions should be followed during this step, including wearing masks, protective glasses, and rubber gloves.
15. Transfer the spent $LiMn_2O_4$ cathode powder to the prepared NaOH solution and stirred to remove impurities, such as residual current collector debris. During the stirring process, the solid:liquid ratio is ~1:25, and the mixture is stirred at 500 rpm for 6 h.
16. Separate the powder and treated liquid by suction filtration and then wash three times with deionized water to completely remove the residual alkali solution. Except for the change of washing reagents, the operation process is the same as described in Step 12.
17. Transfer the treated cathode powder to a blast oven at 100 °C and leave it there until it is completely dry.
18. Collect all pretreated spent $LiMn_2O_4$ cathode powder and transfer it to a drying room or glove box for storage.
    ■ **PAUSE POINT** Cathode materials readily absorb moisture, leading to hydrolysis reactions that generate surface impurities such as residual lithium and promote powder agglomeration. These materials may also react with O_2 and CO_2. This issue is particularly pronounced in spent cathode powders that, due to elemental loss and structural degradation, are more susceptible to reactions with H_2O and CO_2, potentially resulting in phenomena such as proton intercalation. Such reactions hinder subsequent direct

regeneration processes, necessitating strict control of storage conditions. These conditions should also be tailored to the specific type of cathode material. For example, lithium iron phosphate is relatively insensitive to moisture and oxygen and can be stored in a standard dry environment for short durations, although long-term storage still requires moisture protection. In contrast, Ni-rich ternary layered oxides are more vulnerable to oxidation and require more stringent storage measures. Shelf life depends on both storage conditions and material type; for most sensitive materials, exposure to ambient air should be limited to no more than 24 h. Direct regeneration is recommended within 1–2 weeks if stored under dry air, or within several months if preserved in an inert atmosphere.

Failure analysis of spent cathode materials

● **TIMING 2 h**

▲ **CRITICAL** To achieve effective direct regeneration or upcycling of spent cathode materials and minimize material waste, it is essential to understand the material's failure state, particularly the extent of lithium loss and the degradation of its phase structure.

19. Weigh 0.3 g of spent $LiMn_2O_4$ cathode material powder using an analytical balance and transfer it to a polytetrafluoroethylene digestion tank.
20. Prepare aqua regia by mixing concentrated hydrochloric acid and concentrated nitric acid in a 3:1 (vol/vol) ratio to digest the sample. The specific operation in this process is to slowly pour one volume of concentrated nitric acid into three volumes of concentrated hydrochloric acid while continuously stirring with a glass rod.
    ▲ **CAUTION** Both reagents are highly corrosive, and the chlorine gas they emit is toxic, making vapor contact extremely dangerous. Always conduct the preparation process in a fume hood and wear strong acid-resistant rubber gloves, masks and protective glasses.
21. Slowly add 3 mL of concentrated aqua regia to the polytetrafluoroethylene digestion tank and securely cap it.
22. Place the polytetrafluoroethylene digestion tank into the sleeve position of the rotor frame, insert the frame into the microwave digester and connect the temperature sensor.
23. Set the digestion program and start the microwave digestion process. Configure the temperature to 120 °C, the heating time to 5 min and the digestion time to 15 min.
    ▲ **CAUTION** Microwave digestion instruments emit microwave radiation during operation, which can pose health risks if used improperly or for extended periods. They also generate high pressures and temperatures, and in the event of equipment failure or operator error, explosions, fires or other hazardous situations may occur.
24. After completing digestion, remove the rotor frame and place it on a rotatable base inside a fume hood. Use a cap screwdriver to unscrew the pressure relief module, then remove the polytetrafluoroethylene digestion tank from the sleeve.
    ▲ **CAUTION** Remove the rotor frame only after the microwave digester cavity has sufficiently cooled to prevent risks such as burns to the experimenters or overpressure in the digestion tank.
25. Unscrew the digestion tank cap and check if the solution is clear and transparent to confirm that digestion is complete. Once confirmed, rinse any sample residue on the cap with deionized water and return it to the tank.
26. Transfer the digestion solution into a 50 mL volumetric flask. Rinse the digestion tank multiple times with small amounts of deionized water and combine the rinses in the flask. Dilute the solution to the mark with deionized water and mix thoroughly. This solution serves as the major element analysis solution.
27. Start the ICP–OES equipment and ensure the gas cylinder pressure meets the standard. Turn on the Ar gas and exhaust switches, then purge the system for 20 min.
28. Tighten the peristaltic pump tube, turn on the circulating cooling water. Ignite the plasma once the detector temperature reaches −40 °C.
29. Preheat for 10 min, then set the experimental method and configure the parameters for the test elements, conditions and standards.
30. Measure the spectral intensity of each element in a series of standard solutions with varying concentrations and plot a standard curve.

31. Introduce the blank solution and the sample solution into the ICP–OES equipment for analysis. Measure the spectral intensity of each element in both solutions, and calculate the element concentration from the working curve.
▲ **CRITICAL STEP** Analyzing the deficiency of various elements, especially Li, in the cathode material powder after cycling is a critical step in direct recycling, because it influences the choice of recycling method and the amount of reagents required.
32. Calculate the content of each element and the ratio using the formula:

$$w = \frac{(\rho 1 - \rho 0) \times V \times f}{m}$$

where w is the element content; $\rho 1$ and $\rho 0$ are the concentrations of the element in the test and blank solutions, respectively; V is the volume of the test solution; f is the dilution factor; and m is the mass of the sample.
▲ **CRITICAL STEP** ICP–OES typically analyzes the relative proportions of various elements. When assessing the loss of elements in failed cathode powder, it is generally assumed that Li loss is substantially greater than that of other transition metals. As a result, the total amount of transition metals or the content of a specific transition metal is often used as a benchmark to estimate the relative content of Li and other elements. However, it is important to note that the dissolution of transition metal ions is also an intrinsic failure behavior of cathode materials[55,56], which may lead to an underestimate of Li loss. Nevertheless, the error resulting from this underestimation is usually within an acceptable range, as the subsequent lithium replenishment process typically uses a substantial excess of lithium.
◆ **TROUBLESHOOTING**
33. Clean the amorphous glass sample stage, slide and medicine spoon with anhydrous ethanol to remove contaminants, then dry them by blowing with an ear bulb.
34. Turn on the XRD equipment and the circulating cooling water system. Activate the high-voltage generator, set the voltage, current and other parameters, and wait for the equipment to reach the specified power.
35. Use a laboratory spoon to transfer the powder sample into the depression of the amorphous glass sample stage. Spread the sample evenly with a glass slide and press it to create a smooth plane. Remove any excess powder from the sample stage.
▲ **CRITICAL STEP** During sample preparation, the powder sample should completely fill the depressions in the amorphous glass sample stage, ensuring the sample plane is level with the stage to maximize reflected X-rays and achieve a more accurate XRD diffraction pattern.
36. Install the glass sample stage in the designated position of the XRD diffractometer. Adjust the stage so that the sample is aligned with the center of the X-ray beam, then tighten the stage and close the test chamber door.
37. Set the test parameters: the 2θ angle range to 10°–80°, the step size to 0.01°, and the time per step to 0.2 s. Use Cu Kα1 radiation (λ = 1.5406 Å) for XRD measurements.
▲ **CAUTION** X-rays are highly harmful and can pose serious health risks. Never open the protective cover door during the experiment. Take precautions to prevent direct exposure to X-rays and, if possible, wear protective equipment to minimize radiation exposure.
▲ **CRITICAL STEP** To improve data quality and reduce background noise, XRD data that require refinement are typically collected using a slow scan method, which involves reducing the step size and extending the collection time per step.
38. Once the measurement is complete, open the test chamber door and recover the samples.
39. Analyse the collected XRD data for phase identification and use the FullProf program for refinement to extract information such as unit cell parameters, atomic occupancy and defect levels. Use this information to evaluate the material's failure state.
◆ **TROUBLESHOOTING**
40. On the basis of the results of a basic failure analysis of the spent cathode material powder, assess the degree of material degradation. Use this information to select an appropriate direct regeneration method and determine the amount of lithium salt required.

Table 3 | The proportion of primary materials used in various direct regeneration and upcycling processes

Number	Regeneration method	Target product	Lithium salt used to repair Li defects	Li_2CO_3 used for Upcycling	NiO used for Upcycling
1	Solid-phase regeneration	$LiMn_2O_4$	2–3 times the element molar ratio of the actual Li loss	–	–
2	Joule heat-assisted regeneration	$LiMn_2O_4$	1.2–1.5 times the element molar ratio of the actual Li loss	–	–
3		$LiNi_{0.5}Mn_{1.5}O_4$		1/6	2/3
4		$Li_{1.2}Ni_{0.2}Mn_{0.6}O_2$		3/2	2/3

Note that all four procedures use the same starting material. The numbers presented in the table are the molar feed ratios of each reagent, calculated with the spent cathode materials set as the statistical baseline. For example, 2/3 means that the molar ratio of reagent to spent cathode material is 2:3.

Direct regeneration and upcycling of spent cathode materials

● **TIMING 35 h or 5 h**

▲ **CRITICAL** On the basis of the type and degree of failure of spent cathode materials, common direct regeneration methods include solid-phase sintering[28–30], hydrothermal-assisted regeneration[31,32], molten salt-assisted regeneration[33,34,46] and solution lithiation regeneration[35,36]. Relevant references outline the general operation procedures for each method. Here, we describe the most basic solid-phase sintering regeneration (Steps 41–56) and the novel Joule heat-assisted ultrafast regeneration (Steps 57–70), using them as examples to illustrate the specific operational procedures. More importantly, the direct regeneration method is scalable and highly versatile. By harnessing the abundant intrinsic defects in spent cathode materials and designing effective pathways, it can be directly upcycled into a new cathode material for the next generation of LIBs[28,46,48]. A third option is to perform upcycling, and we exemplify this by describing direct upcycling of spent $LiMn_2O_4$ cathode material into high-voltage spinel cathode material $LiNi_{0.5}Mn_{1.5}O_4$ (Steps 71–73), as well as high-energy density, cobalt-free lithium-rich manganese-based cathode material $Li_{1.2}Ni_{0.2}Mn_{0.6}O_2$ (Steps 74–76). The raw material molar ratios used in the experiment are presented in Table 3.

Solid-phase sintering regeneration

41. Weigh a specific amount of spent $LiMn_2O_4$ cathode material powder and transfer it to the preprepared agate ball mill tank.
42. On the basis of the Li loss calculated from the ICP test, weigh the lithium salt corresponding to two to three times the element molar ratio of the actual Li loss. Add the weighed lithium salt into the agate ball mill tank. LiOH and Li_2CO_3 are the most commonly used lithium sources and are broadly applicable to most solid-phase regeneration processes. However, Li_2CO_3 may not be suitable for certain materials, such as Ni-rich layered oxide cathodes, due to phase instability or poor reactivity at low temperatures. In addition to these two lithium salts, other lithium salts or combinations thereof can also be selected for direct regeneration, often providing specific functional advantages, such as enhanced surface modification, altered phase transformation behavior or improved lithium diffusion kinetics. For example, (1) CH_3COOLi can alter the phase transformation pathway during regeneration, (2) Some organic lithium salts, such as 3,4-dihydroxybenzonitrile dilithium, can decompose into functional surface species, promoting surface reconstruction, (3) LiI has been reported to lower the lithiation temperature, which can be advantageous in temperature-sensitive systems. So, lithium salt selection is guided by both material compatibility and functional objectives in the regeneration process.
    ▲ **CRITICAL STEP** Excess lithium salt is crucial in most direct regeneration processes due to differences in the intrinsic structural evolution between direct synthesis and direct regeneration. At lower temperatures, the degradation of the surface structure of the spent cathode material slows the overall lithium replenishment kinetics of the exogenous lithium salt. This leads to a decrease in the conversion and insertion of Li sources under thermal action and an increase in Li source burnout. To achieve sufficient lithium replenishment,

there are two main approaches: (1) enhance lithium replenishment kinetics by improving interfacial lithium salt adsorption, optimizing surface structure reconstruction and adjusting the reaction equilibrium state[37] and (2) compensate for the excessive Li source burnout by using an excess of lithium salts.
As the scale of single direct regeneration of spent cathode materials increases, such as from gram scale in the laboratory to kilogram scale in industry, the proportion of Li source burnout decreases, allowing for a reduction in overall usage of Li salt. In addition, according to experience, the required amount of excess lithium salt varies by cathode material type: layered oxides typically require the highest excess, spinel materials require a moderate amount and olivine materials require the least.

43. Gradually introduce anhydrous ethanol as a grinding aid, maintaining a powder to ethanol mass ratio of 1:2.
44. Add zirconia grinding beads to the agate ball mill tank as grinding media at a powder to grinding beads mass ratio of 1:3. Distribute the grinding beads as follows: 30% large, 50% medium and 20% small beads.
▲ **CAUTION** To ensure safety during the ball milling process, the total volume of grinding beads and material should not exceed 80% of the ball mill tank's capacity. A fill ratio of 40–60% is typically optimal.
45. Install an equal number of preweighed ball mill tanks into the diagonal positions of the planetary ball mill. Secure all the tanks by rotating the spiral buckle, then close the hatch.
▲ **CAUTION** Before starting ball milling, ensure that the ball mill tanks at the diagonal positions are balanced in weight and securely fixed. This prevents potential dangers, such as mechanical failure or material being thrown out due to center imbalance during the milling process.
46. Set up a brief program to run the ball mill at the experimental speed for a few minutes. Observe its operation closely, paying special attention to any unusual sounds, such as loose buckles, to ensure the ball mill is functioning normally.
47. Set the ball milling program according to the experimental conditions: adjust the speed to 400 rpm, set the total milling time to 4 h and alternate between forward and reverse rotation every 15 min.
▲ **CAUTION** During ball mill operation, the high-speed rotation and vibration can cause mechanical parts to wear, loosen or even break. As a result, objects may be ejected with substantial force, posing a safety risk. If you notice unusual sounds or vibrations, stop the equipment immediately.
48. After the ball milling process is completely stopped, loosen the buckle and remove the ball mill tanks. Observe the powder to ensure it is in a normal condition—fine, evenly dispersed and free of flakes or severe agglomeration. If so, transfer it to the blast oven for drying.
◆ **TROUBLESHOOTING**
49. Scrape the dried powder out of the ball mill tanks. Transfer part of the material to an alumina porcelain boat and store the remaining material in a blast oven for later use.
50. Transfer the alumina porcelain boat to the muffle furnace, position it correctly and close the furnace chamber.
▲ **CRITICAL STEP** When the sintering volume of a single batch is large, avoid tightly packing the powder, as it can negatively impact the quality of the recycled material. To improve airflow, introduce a controlled gas flow path (Supplementary Fig. 6).
51. Set the solid-phase sintering program and activate the heating switch. Set the overall heating rate to 3 °C/min. Raise the temperature to 450 °C and maintain it for 2 h. Then, increase the temperature to 850 °C and hold it for 10 h. Finally, allow the sample to cool naturally to room temperature (30 °C).
▲ **CAUTION** When a muffle furnace operates at high temperatures, flammable materials such as paper or plastic can ignite. Therefore, always inspect the experimental area for such materials before use. During operation, the furnace surface and door become extremely hot, creating a risk of burns if touched. After completing an experiment, allow the furnace to cool fully and wear heat-insulating gloves when removing samples to avoid injury.

▲ **CRITICAL STEP** The specific sintering conditions, such as temperature, atmosphere and time, must be determined on the basis of the type of spent cathode material. Typically, the temperature is set close to or slightly higher than the synthesis temperature of the material. For example, the synthesis temperature of $LiNi_{0.8}Co_{0.1}Mn_{0.1}O_2$ is 720 °C, the sintering temperature during direct regeneration can be moderately increased to 750 °C or even 800 °C.

52. Remove the sintered material and transfer it to a beaker. Add deionized water at a solid-to-liquid ratio of 1:20, and wash for 10–15 min to remove residual lithium salt.
▲ **CRITICAL STEP** To compensate for the substantial loss of lithium from the source caused by slow lithium replenishment kinetics, excess lithium salt was added during the batching process. After solid-phase regeneration, small amounts of this lithium salt may remain. These residues must be removed through additional water washing, as their presence could lead to side reactions during electrochemical testing and affect the material's performance evaluation. In addition, the duration of water washing should be adjusted according to the type of spent cathode material. For certain cathode materials that are highly sensitive to H_2O, the washing time should be minimized to prevent hydrated ion intercalation, which could damage the structure of the cathode material.
In large-scale experiments or industrial applications, the test solution from product washing can be reused to re-extract lithium salts, reducing material losses and enhancing economic efficiency.
53. Complete the solid–liquid separation by suction filtration and then transfer the washed material powder to a blast oven for drying.
54. Transfer the dried material powder to an agate mortar and add 0.5–2% LiOH based on the mass ratio. The purpose of adding lithium salt at this stage is to compensate for partial lithium loss that may occur during the preceding water washing process. Such lithium deficiency can lead to partial thermal decomposition of the material at high temperatures, ultimately degrading the performance of the recycled product. The required amount of lithium salt depends on the material type, its reactivity during washing and the re-sintering temperature. For ternary layered oxide cathode materials, which are more sensitive to lithium loss, a higher compensation level—typically 1–2% LiOH by mass—is recommended. In contrast, spinel- and olivine-type cathodes, which exhibit greater structural stability, generally require a lower addition of ~0.5%.
55. Grind the mixture carefully by hand for 20 min until the lithium salt and regenerated cathode material powder are fully and evenly mixed. Then, transfer the mixture to an alumina porcelain boat and place it in a muffle furnace for re-sintering.
56. Set the re-sintering program to heat up to 850 °C at a heating rate of 3 °C/min and maintain it for 2 h and activate the heating switch. Store the powder for subsequent testing.

Joule heat-assisted ultrafast regeneration

57. Follow Steps 43–49 to complete the batching and uniform mixing. The only difference is that less lithium salt is used; use 1.2–1.5 times the intrinsic lithium deficiency of the material.
58. Clean the quartz tube used in the Joule heating experiment with anhydrous ethanol, then dry it with a hair dryer.
59. Place a 0.05-mm-thick layer of graphite paper at the bottom of the tube, and secure it to the tube's mouth using copper foil tape (Supplementary Fig. 7). If graphite paper is unavailable or the operation is considered too cumbersome, the carbon sample tube provided by the Joule heating equipment manufacturer can be used as an alternative.
▲ **CRITICAL STEP** Although spent cathode material powder has inherent conductivity (it typically contains 2–5 wt% conductive carbon, and some industrial-grade cathode material black mass may even include a proportion of spent graphite anode powder), it is difficult to ensure that all particles maintain a conductive network after the initial pretreatment and mixing with exogenous lithium salts. To achieve more uniform energy distribution and heating of the powder, and to avoid introducing additional conductive agents that might affect the final product, using graphite paper is an effective solution.

60. Weigh a specific amount of the preprepared spent cathode material powder and lithium salt mixture. The maximum laboratory scale typically does not exceed 1 g, with the exact amount determined by the size of the quartz tube and equipment parameters.
61. Install a conductive graphite plug at one end of the quartz tube. Load the mixed reactant powder from the other end, then install another conductive graphite plug to create a relatively sealed tubular reaction space. Weigh and record the mass.
62. Tighten the nut, secure the quartz tube onto the Joule heat reaction rack and place the entire assembly into the reaction chamber.
63. Connect the positive and negative wires in the chamber to the corresponding terminals at both ends of the Joule heat reaction rack.
64. Adjust the position of the Joule heat reaction rack so that the reactants in the quartz tube align with the infrared temperature sensor probe.
65. Close the door of the Joule heating equipment's reaction chamber (refer to Supplementary Fig. 8 for a photo of the device). Turn on the current and verify that the current, voltage and resistance values are within a reasonable range. Ensure that the electrodes are properly connected and in contact with the powder, while avoiding short circuits or open circuits.
66. Rotate the temperature sensor control knob on the operation panel to select the high-temperature sensor, and adjust the voltage control knob to set the voltage to 30 V and adjust the current control knob to set the current to 70 A.
    ▲ **CRITICAL STEP** The set voltage and current can influence the heating up time during the sintering process, the higher the value of voltage and current set, the faster the temperature rises. It is necessary to gradually adjust the voltage and current through the experimental results.
67. Set the Joule heating experiment parameters on the main control screen:
    - Select temperature control mode to control the sintering process as the pulsed Joule heating mode
    - Set the target temperature to 1,000 °C
    - Specify one to three pulses. The number of pulses should be optimized on the basis of the specific material and degradation level. It is recommended to examine the material after each pulse to determine whether the desired level of repair has been achieved before proceeding further

      ▲ **CRITICAL STEP** Another control mode is the time control mode, which performs Joule heating sintering for a specified duration. During the process, the temperature fluctuates according to the mold resistance and variations in system current and voltage. While the temperature control is less precise than in temperature control mode, this mode is still suitable for Joule heating experiments and can be selected in other situations.
68. Click the 'Start' button on the main control screen to initiate the Joule heating reaction according to the programmed settings. The system will control the energization and de-energization following the set process. During the sintering process, if you change the automatic process to manual process, you can monitor the reaction voltage, current and temperature on the data trend page. As the temperature rises rapidly, the reactants will first emit yellow light and then transition to a bright white light (Supplementary Fig. 9).
    ▲ **CAUTION** The reaction process involves the use of high voltage and current, which can be hazardous. Although equipment manufacturers have minimized potential risks by integrating electronic circuits and designing protective enclosures, experimenters must still take necessary precautions to prevent accidents, such as explosions, due to circuit failures or excessive transient reactions.
    ◆ **TROUBLESHOOTING**
69. After the reaction is complete, wait for the temperature in the reaction chamber to decrease. Once it has cooled, put on asbestos gloves, unplug the wires from both ends of the Joule heat reaction rack, loosen the nuts and carefully remove the reaction tube. Weigh the sample and record the data.
    ▲ **CAUTION** Some models of Joule heating equipment only record dynamic temperature changes during the operation of the reaction program. Once the reaction is complete, the temperature recording stops. However, the temperature in the chamber may still exceed

safe limits for human skin. Therefore, always wait for the chamber to cool down before handling it. Wear asbestos fireproof gloves when accessing the chamber. Additionally, high-temperature reactions can generate large amounts of gas and smoke; ensure the operation is in a well-ventilated environment. Be sure to wear a dust mask when opening the cabin door.

70. Remove the conductive graphite plug from one end of the quartz tube, then push out the reacted powder. Store the powder for subsequent testing.

Direct upcycling of spent $LiMn_2O_4$ into high-voltage cathode material $LiNi_{0.5}Mn_{1.5}O_4$

71. Calculate the amount of additional chemical reagents required for the upcycling process on the basis of the chemical formulas of the spent material and the target upcycled product. The stoichiometric ratio for spent cathode material ($LiMn_2O_4$), nickel source (NiO) and lithium source (Li_2CO_3) is set as presented in Table 3.
72. Complete the batching and uniform mixing as described in Step 57. In addition to adding the necessary Li salt to compensate for Li deficiency as part of the normal Joule heat-assisted direct regeneration process, incorporate the calculated amounts of nickel source and lithium source from Step 71 to complete the upcycling process.
73. Follow Steps 58–70 to achieve upcycling using the pulsed Joule heating method. Adjust the number of pulses between four and eight on the basis of the basic physical properties of the target product and the classical synthesis process. The specific number of pulses should be optimized by the researcher. After each pulse, the material should be evaluated to assess whether the desired level of repair has been achieved—mainly by examining structural features and key performance indicators (initial specific capacity). This assessment should guide whether to continue or stop pulsing.

Direct upcycling of spent $LiMn_2O_4$ into Li-rich Mn-based cathode material $Li_{1.2}Ni_{0.2}Mn_{0.6}O_2$

74. Calculate the amount of additional chemical reagents required for the upcycling process on the basis of the chemical formulas of the spent material and the target upcycled product. The stoichiometric ratio for spent cathode material ($LiMn_2O_4$), nickel source (NiO) and lithium source (Li_2CO_3) is set as presented in Table 3.
75. Follow Step 57 to complete the batching and uniform mixing. In addition to adding the necessary Li salt to compensate for Li deficiency as part of the normal Joule heat-assisted direct regeneration process, incorporate the calculated amounts of nickel source and lithium source from Step 74 to complete the upcycling process.
76. Follow Steps 58–70 to achieve upcycling using the pulsed Joule heating method. Adjust the number of pulses between 6 and 12 on the basis of the basic physical properties of the target product and the classical synthesis process. The criteria for determining the specific number of pulses are the same as those in Step 73.

Regenerated cathode material characterization

● **TIMING 8 h**

▲ **CRITICAL** To evaluate the phase structure and physical properties of the regenerated and upgraded cathode materials, several key characterizations are essential. First, it is recommended to perform ICP–OES testing (Step 79) to verify that the missing elements in the spent cathode material have been replenished before proceeding with other characterizations. Next, use XRD (Step 80) and SEM (Steps 81–89) to confirm the phase structure and morphological evolution of the material. High-resolution TEM (HRTEM) (Steps 90–98) is used to assess the material's structure and local defects at the atomic scale. Additionally, EPR (Steps 99–103) can compare how different regeneration processes affect the intrinsic defects in the material.

77. PerformICP–OES according to Steps 19–32 to confirm the content of key elements and compare the results with those of the spent materials and commercial materials.
78. Perform XRD according to Steps 33–39 to confirm the phase structure of the regenerated and upgraded material. Then, compare the refined parameters with those of the spent materials and commercial materials.

SEM

79. Cut the Si/SiO_2 wafer into 5 × 5 mm pieces, soak them in anhydrous ethanol, and treat them ultrasonically for ~5 min.
80. Dry the cleaned wafer and use an ear bulb to blow away the contaminants.
81. Weigh ~0.2 mg of the cathode material sample, transfer it into a sample tube and add anhydrous ethanol at a solid-liquid ratio of 1:5.
82. Sonicate the sample tube for 10 min to form a suspension.
    ▲ **CRITICAL STEP** Do not shake the sample tube after sonication to avoid reaggregation of the dispersed particles.
83. Dropcast 10 µL of the cathode material dispersion onto the wafer with a pipette. Turn on the baking lamp to evaporate the ethanol and dry the wafer.
    ▲ **CRITICAL STEP** Check carefully to ensure that the suspension is added to the front (bright) side of the chip before proceeding.
84. Paste the wafer onto a suitable sample stage using conductive tape or attach the electrode sheet or cathode material powder directly onto the conductive tape, depending on the test target.
    ▲ **CAUTION** Ensure that the sample stage is the correct size for the instrument, paying particular attention to the overall height after the wafer is pasted on. This will prevent any potential damage to the equipment or obstruction of the lens during sampling.
85. Wear gloves, assemble the sample stage into the corresponding position in the SEM equipment, close the door and evacuate the chamber to the required vacuum level.
86. Adjust the sample stage to the appropriate height, turn on the electron beam, and set the accelerating voltage within the range of 3–10 kV. Activate the image acquisition function and capture images of the sample at various magnifications by adjusting parameters such as magnification, focus and contrast.
    ◆ **TROUBLESHOOTING**
87. Increase the device's acceleration voltage to 12–15 kV, activate the EDS plug-in and perform energy spectrum analysis using point scan, line scan and surface scan techniques.

HRTEM

88. Prepare the sample suspension as described in Steps 83–84.
89. Dropcast 10 µL of the cathode material dispersion onto the ultrathin carbon film copper mesh or micro-grid copper mesh with a pipette. Turn on the baking lamp to evaporate the ethanol and dry the copper mesh.
90. Remove the sleeve from the front end of the TEM sample rod, unscrew the sample fixation nut using a small slotted screwdriver and remove the small beryllium ring using a tweezer.
91. Place the copper mesh face down into the O-ring of the sample rod, carefully position the small beryllium ring on the mesh, align its protruding part with the corresponding groove in the sample rod and then secure the fixing nut with a slotted screwdriver.
    ▲ **CAUTION** (1) The sample rod is a highly delicate component of the instrument. Handle it with care and gentleness, avoiding any rough handling. Do not touch any part of the sample rod, from the O-ring to the top, with your hands. (2) Before testing, ensure that the sample is nonmagnetic to prevent it from being ejected and adhering to the objective lens pole shoe due to the magnetic field during the test. (3) Exercise special caution when handling the small beryllium ring, as it is toxic. Never touch it with your bare hands.
92. Operate the TEM equipment to ensure that the coordinates of each sample are set to zero. Align the limit pin with the Cose mark, then carefully insert the sample rod parallel to the axis. Slide the sample rod inward until it encounters an obstacle, triggering the pre-evacuation of the sample chamber.
93. Wait for the pre-evacuation to complete, then begin the injection process when the indicator light signals. During this procedure, hold the end of the sample rod and rotate it 90° counterclockwise around the axis. Align the sample rod pin with the round hole on the sample stage, then allow the sample rod to slowly slide into the TEM device under the vacuum suction, positioning it at the bottom. While injecting the sample, monitor the vacuum value to ensure it remains within the normal range.

▲ **CAUTION** When inserting the sample rod, handle it gently and avoid twisting it forcefully to prevent it from hitting the sample stage.

94. Adjust the height and position of the sample stage to align with the desired observation area. Set the test voltage to 300 kV and align the electron optical path system to ensure proper axis alignment.
95. Locate the appropriate characterization area, activate the image acquisition function, and capture sample images at various magnifications. Adjust parameters such as magnification, focal length, astigmatism and contrast to optimize the images.
◆ **TROUBLESHOOTING**
96. Adjust the equipment's aperture and active the specific plug-in and perform energy spectrum, electron loss energy spectrum, electron diffraction and other analyses.

EPR

97. Grind the cathode material powder to prevent agglomeration and sieve it to remove large particles. Then, place the powder sample into a dedicated quartz tube, seal it and evacuate for testing.
98. Turn on the EPR instrument and preheat it for ~10 min.
99. Set the magnetic field scanning range and scanning rate, and select the appropriate band, modulation frequency and amplitude.
100. Remove the dustproof cover from the instrument test port and place the sealed quartz tube sample into the EPR chamber.
101. Start the scan on the basis of the set conditions, record the EPR spectrum and measure the spectral line intensity and *g*-factor.
▲ **CRITICAL STEP** Different samples may require distinct scanning parameters and quantitative methods, which should be optimized on the basis of the specific conditions. During the measurement, maintain a stable instrument environment to prevent interference from magnetic fields and temperature fluctuations.

Electrochemical performance verification

● **TIMING 30–40 d**

102. Weigh 2 g of PVDF into a small glass bottle, add NMP at a solid-to-liquid ratio of 1:25, place a magnetic stirrer inside, tightly seal the bottle and stir at 500 rpm for 24 h.
▲ **CAUTION** NMP is volatile and irritating. During operation, should avoid contact with skin and eyes, inhalation, and exposure to fire.
▲ **CRITICAL STEP** To achieve more uniform dissolution and dispersion of PVDF in NMP, you can choose to flip the glass bottle and continue stirring after 12 h of initial stirring.
103. Weigh 200 mg of cathode material powder and 25 mg of acetylene black. Add them to an agate mortar and grind manually for 15 min to achieve an initial mix.
▲ **CAUTION** Acetylene black powder is very light and tends to float during the early stages of grinding. Experimenters should wear dust masks to avoid inhalation into the mouth and nose.
▲ **CRITICAL STEP** Conduct the related experiments in a drying room to prevent moisture absorption from the air, which could affect the slurry's performance. If the laboratory humidity is high, grind the mixture under a baking lamp and then dry it in a blast oven for 10–15 min before proceeding with subsequent operations.
104. Transfer the mixed powder to a dedicated plastic jar. Add the preprepared PVDF–NMP solution dropwise, maintaining a mass ratio of cathode material to PVDF of 8:1.
▲ **CRITICAL STEP** When adding the drops, control both the speed and position of the addition to prevent local slurry agglomeration or premature gelation.
105. Place the dedicated plastic jar into the corresponding slurry defoaming machine, close the door and homogenize the mixture for 6 min according to the program.
▲ **CAUTION** Ensure the slurry in the plastic jar does not exceed the recommended capacity, as overloading can lead to overheating or reduced performance. Do not place any objects on the platform or allow foreign matter to enter openings in the main

machine, as this may cause errors or equipment failure. Additionally, avoid prolonged operation and allow the machine to cool down to prevent overheating.

106. Take the plastic jar out and observe slurry consistency. If necessary, add more NMP to adjust the viscosity, then return the slurry to the homogenizer and homogenize it for 8 min to complete the slurry preparation.
◆ **TROUBLESHOOTING**

107. Spray a small amount of anhydrous ethanol onto the surface, use a vacuum suction cup to adsorb the Al foil onto the coating machine and then wipe the surface of the Al foil with anhydrous ethanol to remove any adsorbed dust.

108. In this protocol, a 200 μm coating scraper is typically used for applying the slurry to the aluminum foil. Position the coating scraper parallel to one end of the Al foil, then use the coating machine to push the scraper at a constant speed, ensuring an even application of the mixed slurry onto the Al foil.
▲ **CAUTION** Operate it inside a fume hood to facilitate the extraction and adsorption of a large amount of volatile organic solvents. Always wear appropriate protective equipment when handling it, avoid contact with skin and eyes and prevent inhalation of vapors and fumes.
◆ **TROUBLESHOOTING**

109. Transfer the Al foil with the coated slurry into a vacuum blast oven and dry it at 90 °C for 8 h.

110. Clamp the Al foil coated with cathode material using weighing paper, and use a cutting machine to cut it into Φ12 diameter discs as cathode electrodes. Then, transfer the discs to a glove box or vacuum storage box for later use.
▲ **CAUTION** During the experiment, take care to avoid injuring your fingers with the cutting machine.

111. Prepare the various components required for battery assembly and bring them into a glove box filled with argon to assemble the half cell.
▲ **CAUTION** It is best to dry the items in a blast oven before bringing them into the glove box. Additionally, in order not to pollute the atmosphere inside the glovebox (H_2O <0.01 ppm, O_2 <0.01 ppm), any material which is transferred into or out of it needs to pass through an antechamber. After loading a component from the outside into the antechamber, typically a sequence of vacuum/refilling removes air from the antechamber and replaces it with inert gas. Here, we recommend performing at least three vacuum/refill cycles before opening the inner door of the antechamber.

112. Use an analytical balance to weigh the mass of the cathode electrode sheet used in the battery assembly. Calculate the mass of the active material subtracting the mass of the empty aluminum foil and applying the specified active material ratio. In this protocol, the active material loading was maintained between 6 and 8 mg/cm^2.

113. Place the negative electrode shell on the dust-free paper. Then, put in the Li metal sheet (Φ14) and use a pipette to add 25 μL of electrolyte.

114. Next, place a polypropylene diaphragm with a diameter of Φ16 and use a pipette to add 25 μL of electrolyte again.

115. Carefully position the cathode electrode sheet at the center of the diaphragm, then sequentially put in a Φ14 stainless-steel gasket and shrapnel. Finally, cover the assembly with the positive electrode shell.

116. Use insulated tweezers to place the assembled battery, with the negative electrode side facing up, onto the button battery sealing machine mold. Adjust the pressure (typically 800 Pa) and press for 5 s to complete the assembly and preparation of the button battery.
▲ **CRITICAL STEP** The pressing pressure depends on the model of the sealing machine and the appropriate pressure should be confirmed on the basis of experience. Excessive pressure may deform the battery or even cause a short circuit, while insufficient pressure could lead to a loosely packaged battery, allowing air to enter, which may result in Li metal oxidation and electrolyte degradation.

117. Remove the battery using insulated tweezers, check whether the assembly is complete and wipe off any excess electrolyte using dust-free paper.

Table 4 | Basic parameter settings for electrochemical testing of different materials in this protocol

Materials	Voltage range	Nominal specific capacity	Maximum test rate
$LiMn_2O_4$	3.0–4.5 V	148 mAh/g	10 C
$LiNi_{0.5}Mn_{1.5}O_4$	3.5–4.9 V	148 mAh/g	15 C
$Li_{1.2}Ni_{0.2}Mn_{0.6}O_2$	2.0–4.8 V	250 mAh/g	10 C

C-rate (C) is a standard unit that describes the charge or discharge current relative to the battery's nominal capacity.

118. Take out the pressed button battery, check that the open circuit voltage is ~3.0 V and then place it with the negative electrode facing up for ~4 h to allow the electrolyte to thoroughly soak the electrode.
◆ **TROUBLESHOOTING**
119. Connect the assembled button cell to the external fixture of the battery test system, ensuring proper alignment and secure contact between the cell and the fixture.
120. Set the relevant parameters for the electrochemical performance test in the operation terminal on the basis of the characteristics of different cathode materials. These parameters include test type, voltage range, nominal specific capacity, number of cycles and rate range. Refer to Table 4 for the specific parameters used in this protocol.
121. Start the test and observe the electrochemical curves of half cells, assembled with different materials, during the first cycle of charge and discharge at low current density.
◆ **TROUBLESHOOTING**
122. Conduct long-term cycle tests and rate tests as required to evaluate the battery's service life and its ability to charge and discharge rapidly.
▲ **CRITICAL STEP** Ensure that the entire testing process is conducted at a constant temperature (typically 25 °C or 30 °C) to facilitate the comparison for different materials. When necessary, adjust the temperature of the thermostatic chamber to test the high and low temperature performance of recycled materials.
◆ **TROUBLESHOOTING**

Troubleshooting

Troubleshooting advice can be found in Table 5.

Table 5 | Troubleshooting

Step	Problem	Possible reason	Possible solution
8	Residual silver–white metal debris is present in the collected spent cathode material powder	Improper handling during the separation of spent cathode material powder from the current collector resulted in Al foil debris detaching and remaining	(1) Control the treatment time and intensity during the separation process. (2) Screen to remove large pieces of debris and further eliminate residual Al foil debris by post-treatment with NaOH solution
8	The structure of the spent cathode material undergoes an unexpected phase change after separation	The separation method is incompatible with the material system, leading to thermal reduction reactions or reactions with the treatment reagent	Adjust the separation method accordingly
32	Abnormally high lithium loss in spent cathode material as measured by ICP–OES	Incomplete discharge of spent LIBs before disassembly	(1) Ensure that spent LIBs are fully discharged to 1.5 V in Step 3 to prevent incomplete discharge. (2) Add extra lithium salt during the subsequent repair process to compensate for the loss
39	Failure to converge or program errors resulting in termination during XRD refinement	Initial parameter settings may be very different to the actual structural values, or some parameters may fall outside the reasonable range of physical properties	Manually adjust the parameters on the basis of the XRD diffraction pattern, using basic formulas and prior experience to estimate reasonable ranges. Guide the refinement process by expanding parameter limits, adjusting the refinement order and fine-tuning other settings as needed

Table 5 (continued) | Troubleshooting

Step	Problem	Possible reason	Possible solution
48	The powder after wet grinding is flaky, does not appear fine and exhibits substantial agglomeration	Excessive ethanol or an inappropriate ratio of grinding beads during wet grinding may have weakened the interaction between powders, leading to poor grinding efficiency and agglomeration	(1) Reduce the amount of anhydrous ethanol added in Step 43 to avoid excessive dispersion of the powders; (2) Adjust the grinding bead ratio in Step 44, increasing the ratio of smaller beads. (3) Optimize milling time and speed
68	The Joule heating process halts before reaching the set temperature	The material may disperse during heating, or the graphite paper may be damaged, leading to poor contact between the electrode and the material. This limits the current flow, preventing the material from reaching the target temperature	Replace the graphite paper during the sample loading process and adjust the conductive graphite plug to compact the reactant powder, ensuring better electrical contact
86	During the SEM test, abnormally bright or dark alternating stripes appear in the image or the image is deformed and drifts	The sample has poor conductivity, causing free electrons to accumulate locally, forming an electrostatic field that disrupts the normal overflow of electronic information	Before testing, place the sample stage with the attached sample in the coating machine and deposit a thin layer of Au on the sample through sputtering. This will improve conductivity and result in better SEM imaging
95	No clear lattice phase can be observed at the edge of the sample	The cathode material sample particles are too large, preventing the electron beam from penetrating any thin areas at the edge of the particles, which results in the inability to capture a clear lattice phase image	Replace the particles and attempt to locate a thinner area or use FIB milling to thin the sample in advance
95	Some samples melt or undergo phase changes when exposed to the electron beam	The samples may lack stability or be highly sensitive to electron beam exposure	Reduce the acceleration voltage during testing or apply frozen sample preparation techniques to minimize electron beam damage
106	The slurry flocculates and loses fluidity	The slurry absorbs water or the residual alkali on the surface of the cathode material is too high	(1) Control the humidity of the experimental environment to prevent water absorption. (2) Wash and dry the cathode material to remove excess residual alkali on the surface
108	The surface of the slurry is not smooth after coating, and protruding particles appear	The cathode material particles are too large. Or the mixing process is uneven, leading to agglomeration during slurry preparation	(1) Grind the cathode material powder thoroughly before mixing to ensure uniform particle size. (2) Optimize the homogenization process by controlling the experimental environment's humidity, fully grinding during the premixing process, and carefully controlling the speed and position of the drop process to prevent agglomeration
118	The open circuit voltage of the assembled button battery is low	(1) Burrs on the electrode pierce the diaphragm, causing the battery to short circuit. (2) During assembly, the positive and negative electrodes are misaligned or mistakenly connected directly, leading to a short circuit. (3) The battery pressing process is incorrect, resulting in improper contact between the positive and negative electrode shells and electrode sheets, causing a short circuit	(1) Optimize the electrode manufacturing process to reduce burrs and ensure precise alignment of the electrodes. (2) Carefully control the assembly process to ensure correct positioning of the electrodes and prevent any accidental short circuits. (3) Adjust the battery pressing process to ensure proper contact between the electrode shells and electrode sheets, avoiding a short circuit
121	The first-cycle charging capacity of the regenerated material exceeds the standard and the first-cycle coulombic efficiency is low	Excessive residual Li salt on the surface of the regenerated cathode material or side reactions under high voltage	Wash the regenerated cathode material as described in Steps 52–56 and re-sinter it to remove impurities
122	The capacity or cycle performance of the regenerated material is substantially lower than that of the commercial material	The repair process may be incomplete, preventing full restoration of the material	(1) Adjust the amount of lithium salt, regeneration temperature, treatment time or repair method. (2) Supplement the dissolved transition metal with the corresponding raw materials before sintering[34]

Timing

Spent battery disassembly and pretreatment

Step 1, gathering information: ~5 min (depends on the amount of data available before the spent battery is discarded)
Steps 2–4, spent battery discharge: ~12 h
Step 5–6, spent battery disassembly: 15 min
Step 7, spent electrode treatment: 25 min (depends on the electrode type and the amount of single treatment applied)

Step 8, separation of current collector and active material powder: 1 h (depends on the electrode type and separation method)
Steps 9–10, large particle screening and removal: 20 min
Steps 11–13, binder and some impurities removal: 9 h
Steps 14–18, Al foil impurities removal: 9 h

Failure analysis of spent cathode materials

Steps 19–32, ICP–OES measurement: 90 min
Steps 33–39, XRD measurement: 30 min
Steps 33–39, regeneration plan formulation: 10 min

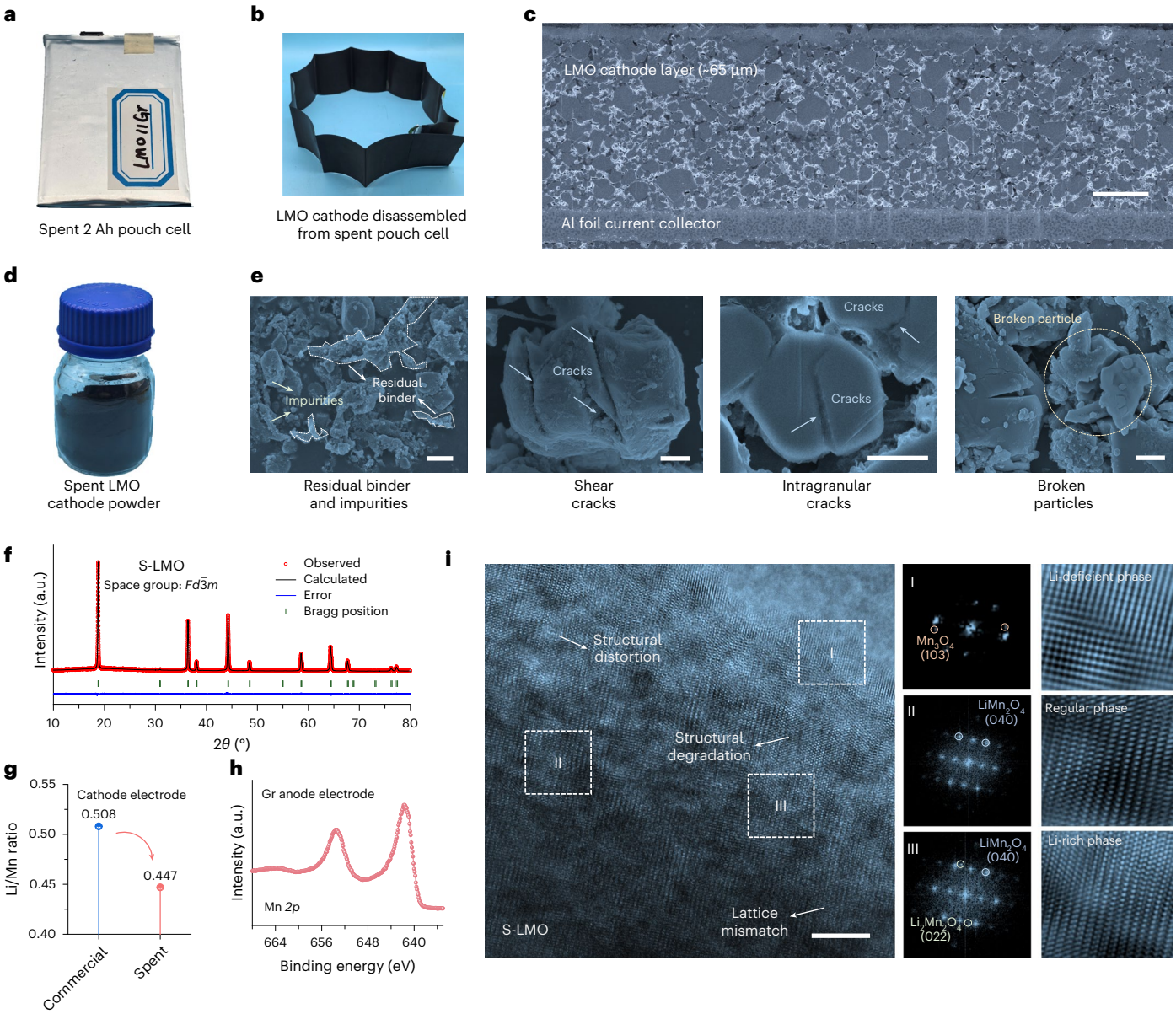

Fig. 3 | Failure analysis of spent cathode materials. a,**b**, Digital photos of the S-LMO pouch cell (**a**) and electrodes (**b**). **c**, An SEM image of the cross section of S-LMO electrode (scale bar, 2 µm). **d**, A digital photo of the S-LMO powder. **e**, SEM images of typical failure characteristics of the cathode material (from left to right: scale bars, 2 µm, 300 nm, 1 µm and 500 nm, respectively). **f**, Rietveld refinement of XRD pattern of S-LMO. **g**, A comparison of Li content in S-LMO and C-LMO analyzed via ICP–OES. **h**, Mn 2*p* XPS spectra collected from the spent Gr anode electrode. **i**, HRTEM analysis of S-LMO (scale bar, 5 nm).

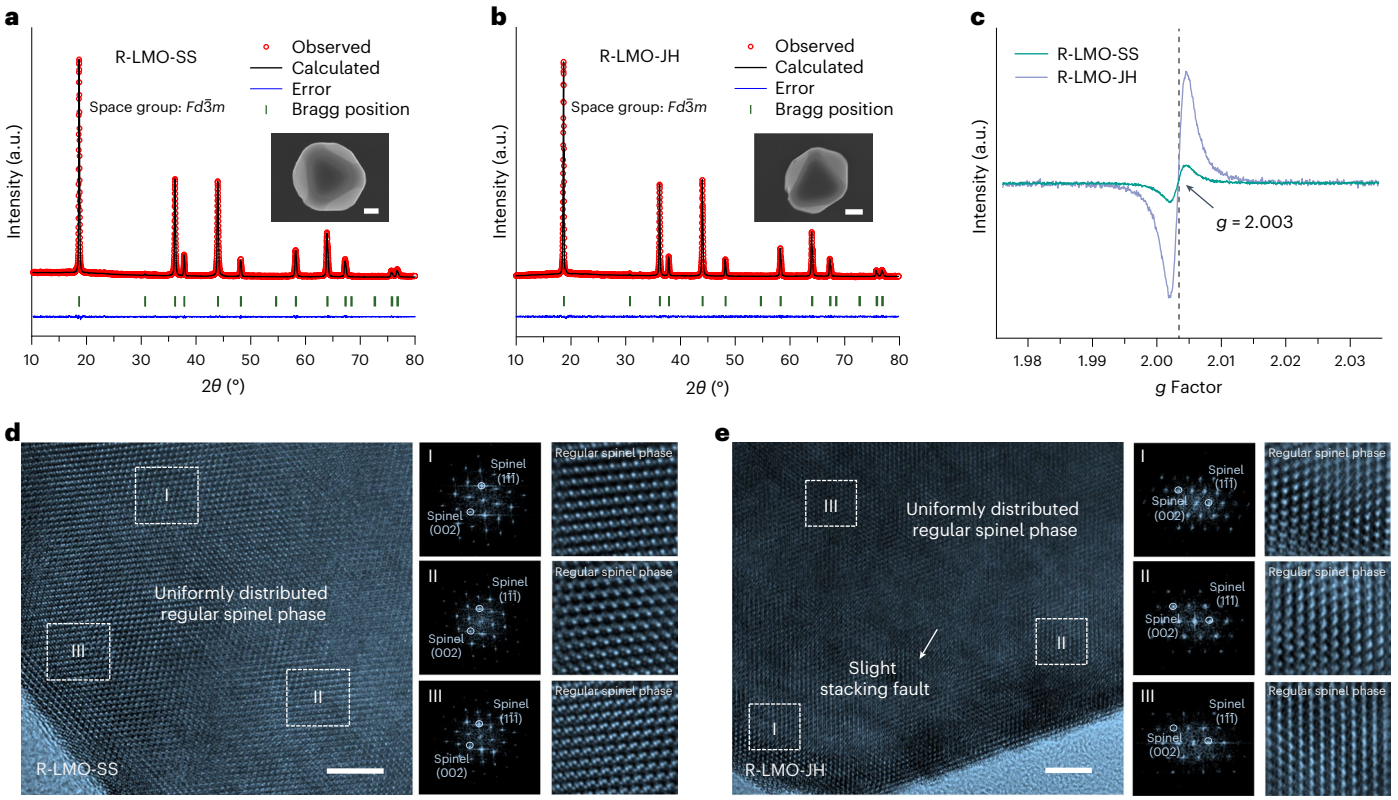

Fig. 4 | Structural characterization of regenerated $LiMn_2O_4$ cathode materials. a,**b**, Rietveld refinement of XRD patterns of R-LMO-SS (**a**) and R-LMO-JH (**b**) (insets, SEM images of R-LMO-SS (**a**) and R-LMO-JH (**b**); scale bars, 100 nm (**a**) and 200 nm (**b**)). **c**, EPR spectrums of R-LMO-SS and R-LMO-JH. **d**,**e**, HRTEM analysis of R-LMO-SS (**d**) and R-LMO-JH (**e**) (scale bars (**d**,**e**), 5 nm).

Direct regeneration and upcycling of spent cathode materials

Steps 41–49 or Steps 57 or Steps 72 or Steps 75, raw material ball milling: 4.5 h
Steps 50–56, solid-phase sintering regeneration: 28 h
Steps 58–70, Joule heat-assisted ultrafast regeneration: 20 min
Step 73, directly upcycle the spent $LiMn_2O_4$ into high-voltage cathode material $LiNi_{0.5}Mn_{1.5}O_4$: 20 min
Steps 76, directly upcycle the spent $LiMn_2O_4$ into Li-rich Mn-based cathode material $Li_{1.2}Ni_{0.2}Mn_{0.6}O_2$: 20 min

Regenerated cathode material characterization

Step 77, ICP–OES measurement: 90 min
Step 78, XRD measurement: 30 min
Steps 79–87, SEM measurement: 2 h
Steps 88–96, TEM measurement: 2.5 h (depends on the specific measurement situation)
Steps 97–101, EPR measurement: 1 h

Electrochemical performance verification

Steps 102–106, slurry preparation: 1 h
Steps 107–108, slurry coating: 5 min
Step 109, electrode drying: 8 h
Step 110, electrode cutting: 10 min
Steps 111–118, half-cell assembly: 30 min
Steps 119–122, electrochemical performance test: 30–40 d (depends on the material type and the test type)

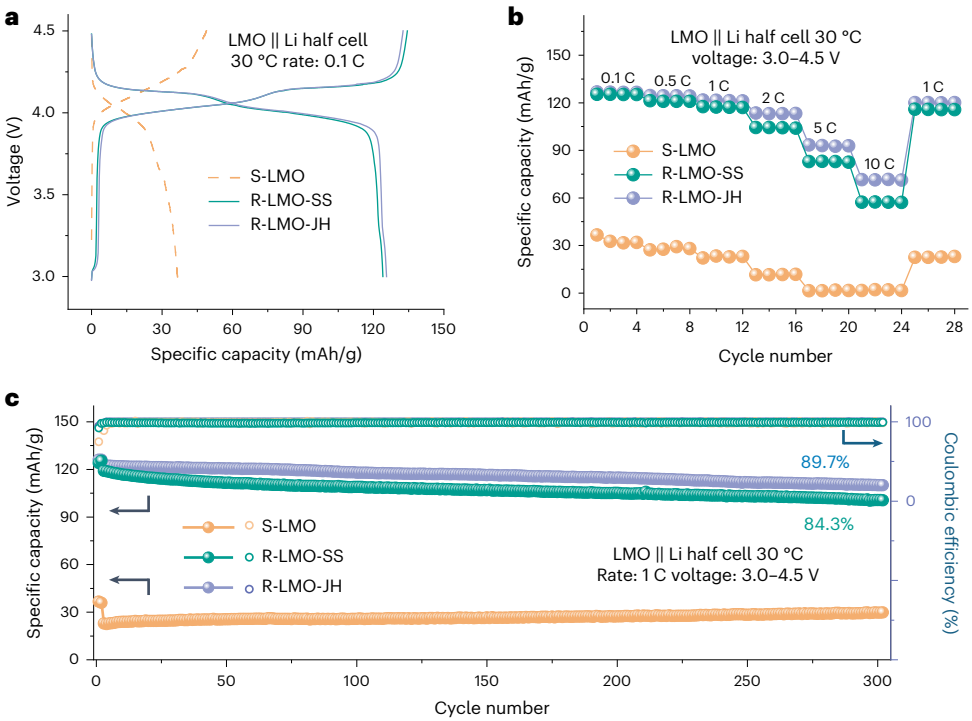

Fig. 5 | Electrochemical performance of regenerated $LiMn_2O_4$ cathode materials. a, Galvanostatic charge/discharge curves of S-LMO, R-LMO-SS and R-LMO-JH in the voltage range of 3.0–4.5 V at 0.1 C. **b**, Cycling performance of S-LMO, R-LMO-SS and R-LMO-JH at 1 C. **c**, Rate performance of S-LMO, R-LMO-SS and R-LMO-JH at various current densities.

Anticipated results

In this section, we use spent $LiMn_2O_4$ as an example to showcase key structural characterization and performance verification results. These results demonstrate that the direct regeneration and upcycling of spent cathode materials can be successfully achieved using this protocol.

Acquisition and failure analysis of spent cathode materials

The spent $LiMn_2O_4$//graphite (LMO//Gr) pouch cell, shown in Fig. 3a, was disassembled to separate its components, including the cathode electrode, anode electrode and separator (Supplementary Fig. 5). The cathode electrode, illustrated in Fig. 3b, features an active material coating evenly applied to both sides of the Al foil current collector. SEM analysis of the cross-section revealed that the cathode material coating on each side was ~65 µm thick, with a high proportion of active material and low porosity (Fig. 3c). Following further separation and pretreatment steps, the cathode material powder needed for the recycling experiment was obtained, labeled as S-LMO (Fig. 3d).

As shown in Fig. 3e, the microscopic morphology of this group of failed cathode materials reveals spherical single crystals with sizes ranging from 1 to 3 µm. After prolonged cycling, typical mechanical failure behaviors are evident, including shear cracks, intergranular cracks and particle breakage. Additionally, the particle surfaces appear relatively rough, probably due to surface damage caused by electrolyte corrosion. Residual binder and side reaction products are also clearly visible. From the perspective of crystal structure, all peaks in the XRD spectrum of the failed material align well with the spinel structure (space group *Fd*3*m*) and no impurity peaks are observed. However, the main peak (111) is noticeably shifted to a higher angle. Refinement analysis reveals that the unit cell parameter has decreased to 8.1856 Å, smaller than the 8.2312 observed in the commercial material (C-LMO) (Fig. 3f, Supplementary Fig. 10 and Supplementary Tables 3 and 4). This reduction confirms a substantial collapse of the material structure, which is a typical characteristic of lithium deficiency in this type

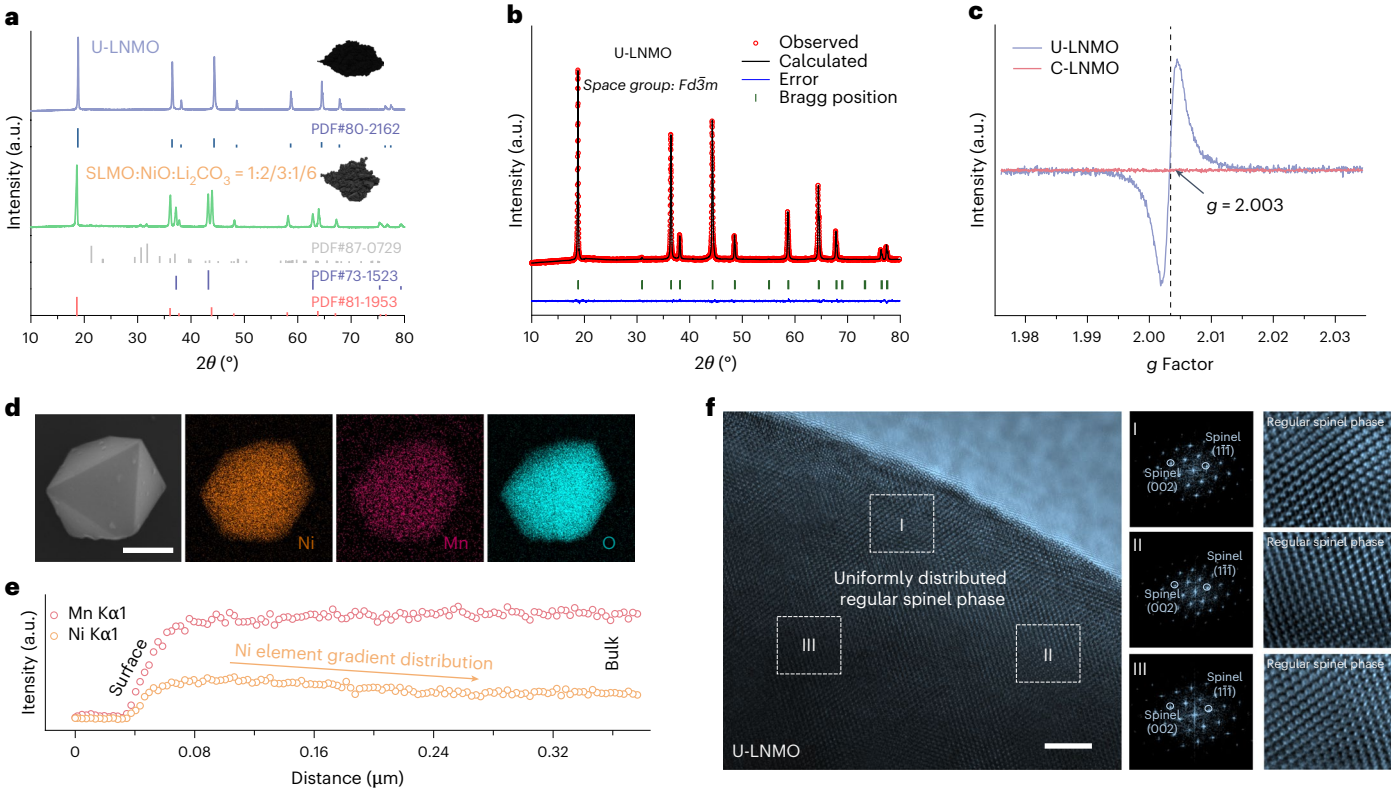

Fig. 6 | Structural characterization of upcycled high-voltage cathode material $LiNi_{0.5}Mn_{1.5}O_4$. **a**, XRD patterns of upcycled precursors and products (powder diffraction file (PDF); insets show digital photos of the corresponding powders). **b**, Rietveld refinement of XRD pattern of U-LNMO. **c**, EPR spectrums of U-LNMO and C-LNMO. **d**, SEM image and EDS mapping of U-LNMO (scale bar, 500 nm). **e**, EDS line scan of the internal section of U-LNMO. **f**, HRTEM analysis of U-LNMO (scale bar, 5 nm).

of material[57]. ICP–OES testing revealed a specific lithium deficiency of 10.6% in the material (Fig. 3g and Supplementary Table 2). Additionally, XPS analysis of the Gr anode electrode detected Mn signals (Fig. 3h), confirming that Mn was also lost from the material due to dissolution[56]. As shown in Fig. 3i and Supplementary Fig. 11, HRTEM was used to conduct a more detailed failure analysis at the microscopic level. The results reveal that, due to Jahn-Teller distortion during the redox process and the irreversible phase evolution driven by Mn^{3+} disproportionation, the material exhibits the formation of a Li-deficient Mn_3O_4 phase and a Li-rich $Li_2Mn_2O_4$ phase after long-term cycling[58,59]. This finding further highlights the uneven distribution of lithium in the spent cathode material.

Direct regeneration of spent cathode materials

After identifying the failure characteristics of the spent cathode material, direct recycling was achieved using solid-phase regeneration and Joule heat ultrafast regeneration methods, designated as R-LMO-SS and R-LMO-JH, respectively. ICP–OES analysis confirmed that both methods effectively replenished the missing Li (Supplementary Table 2). As shown in Fig. 4a,b and Supplementary Tables 5 and 6, the unit cell parameters of the regenerated materials were 8.2326 Å and 8.2311 Å, respectively, indicating successful restoration of the crystal structure and resolution of lattice collapse. After recrystallization and crystal growth during the two kinds of regeneration processes, both regenerated materials exhibit the characteristic octahedral morphology of spinel cathode materials. From a microstructural perspective, the failure phases on the surface of the spent material were completely eliminated, and both regenerated materials exhibited a uniformly distributed conventional spinel structure (Fig. 4d,e). However, the nonequilibrium synthesis process in the Joule heat method led to more structural defects in

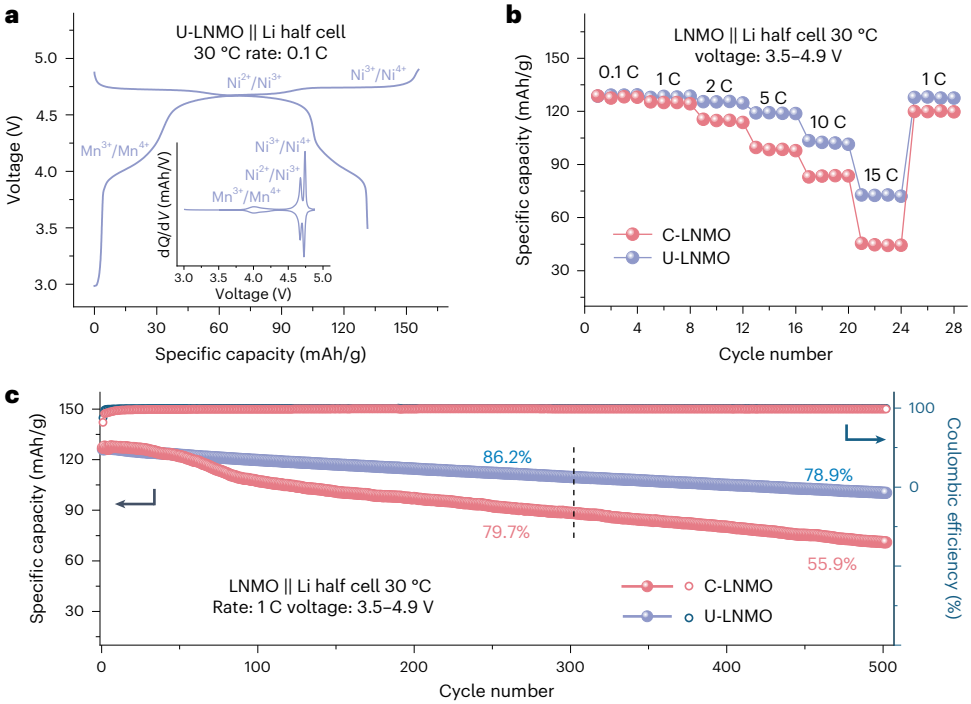

Fig. 7 | Electrochemical performance of upcycled high-voltage cathode material $LiNi_{0.5}Mn_{1.5}O_4$. **a**, Galvanostatic charge/discharge curve of U-LNMO in the voltage range of 3.5–4.9 V at 0.1 C (The inset is the corresponding d*Q*/d*V* curve). **b**, Cycling performance of U-LNMO and C-LNMO at 1 C. **c**, The rate performance of U-LNMO and C-LNMO at various current densities.

R-LMO-JH, including stacking faults and twin boundaries[42,60]. The presence of oxygen vacancies was also confirmed by EPR (Fig. 4c). These structural characteristics were also reflected in the materials' electrochemical properties. The open circuit voltage of S-LMO was ~3.2 V, consistent with its lithium-deficient nature. Additionally, its charge–discharge profile showed severe polarization and a short platform, with Li^+ insertion and deinsertion channels blocked by structural collapse, resulting in a capacity of only 36.6 mAh/g in the first cycle. In contrast, the charge–discharge curves and redox behavior of both regenerated materials returned to normal, delivering capacities of 124 and 125.6 mAh/g, respectively (Fig. 5a and Supplementary Fig. 12). Cycling and rate performance tests further demonstrated that S-LMO was no longer viable for electrochemical operations, while both regenerated materials exhibited performance comparable to C-LMO (Fig. 5b,c and Supplementary Fig. 13). Notably, the nonequilibrium thermochemical process in R-LMO-JH introduced appropriate structural defects[43,61], resulting in superior electrochemical performance. R-LMO-JH retained 89.7% of its capacity after 300 cycles and achieved 71.3 mAh/g at a high current density of 10 C.

Direct upcycling of spent cathode materials into next-generation cathode materials

Direct upcycling of spent $LiMn_2O_4$ into high-voltage cathode material $LiNi_{0.5}Mn_{1.5}O_4$

When a feasible direct phase evolution path exists between the target upcycled material and the initial cathode material, the spent cathode material can be effectively upcycled using the direct regeneration method. As shown in Fig. 6a,b, the direct transformation of S-LMO into the high-voltage cathode material $LiNi_{0.5}Mn_{1.5}O_4$ (U-LNMO) was achieved by uniformly mixing the spent cathode material with a Ni source and Li source in a specific ratio, followed by the Joule heat method. Following this process, the powder color changes from dark brown to black. The change in elemental content confirms the successful completion of Li compensation and Ni insertion (Supplementary Table 2). The crystal structure of U-LNMO retains the spinel configuration, with structural parameters comparable to the commercial material (C-LNMO)

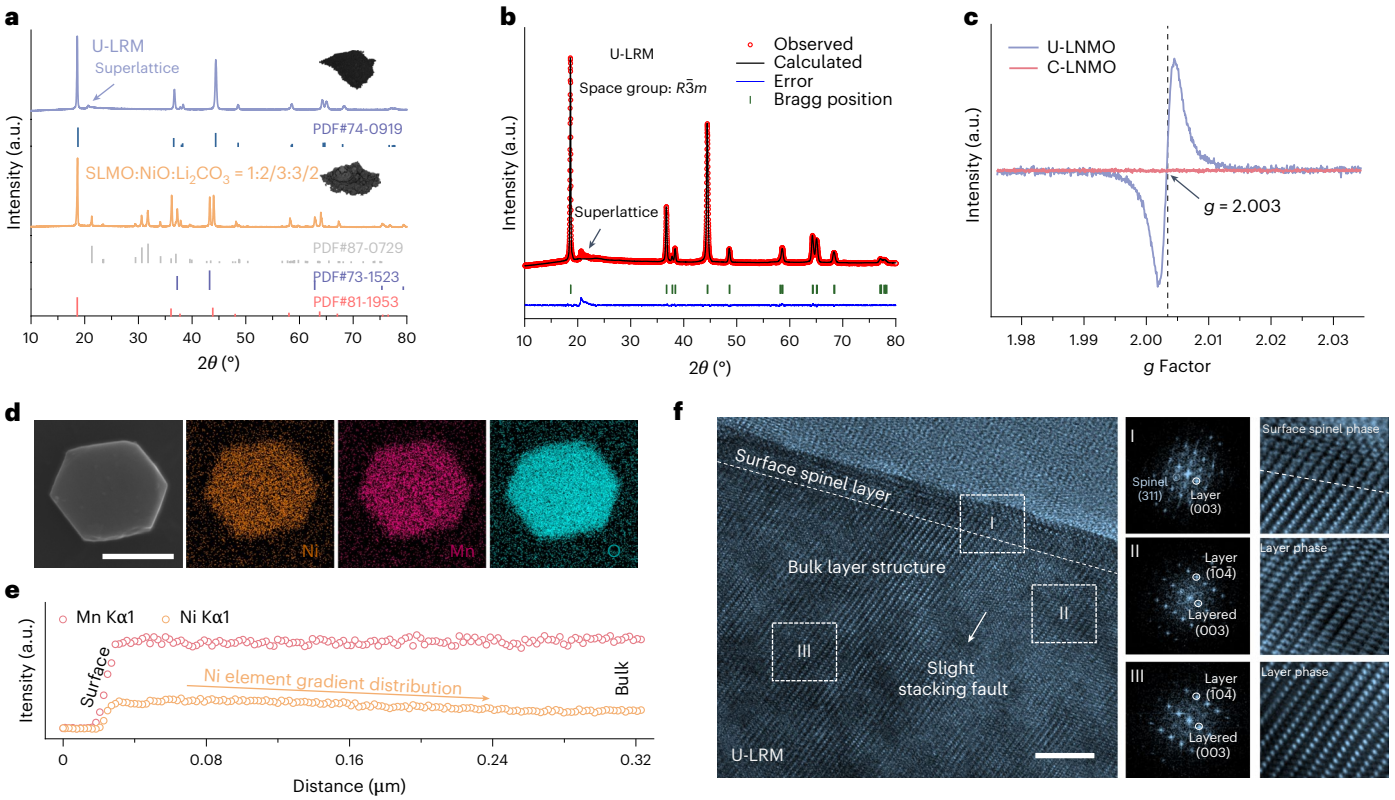

Fig. 8 | Structural characterization of upcycled Li-rich Mn-based cathode material $Li_{1.2}Ni_{0.2}Mn_{0.6}O_2$. a, XRD patterns of upcycled precursors and products (the insets show digital photos of the corresponding powders.) **b**, Rietveld refinement of XRD pattern of U-LRMNMO. **c**, EPR spectrums of U-LRM and C-LRM. **d**, SEM image and EDS mapping of U-LRM (scale bar, 500 nm). **e**, EDS line scan of the internal section of U-LRM. **f**, HRTEM analysis of U-LRM (scale bar, 5 nm).

(Supplementary Fig. 14 and Supplementary Tables 7 and 8). Morphologically, U-LNMO exhibits a typical octahedral shape with sharper edges and corners compared with LMO (Fig. 6d). HRTEM images confirm that U-LNMO has a uniformly distributed spinel structure similar to that of U-LMO (Fig. 6f). The Joule heat method introduces two notable features into U-LNMO. First, as shown in Fig. 6c, the EPR spectrum reveals a strong oxygen vacancy signal in U-LNMO, which is nearly undetectable in C-LNMO. Second, as demonstrated in Fig. 6e, while the surface elemental distribution of Ni is uniform, a gradient distribution of Ni from the surface to the bulk is evident in the line scan analysis. This gradient is attributed to the short heating and cooling times during Joule heating, which limit the homogenization of exogenous Ni atoms, thus forming a natural gradient material. Both features are considered beneficial for the electrochemical performance of the material[62,63]. As seen in the charge–discharge and dQ/dV curves (Fig. 7a), U-LNMO exhibits a distinct high-voltage plateau, delivering an initial capacity of 127 mAh/g. At a high cut-off voltage of 4.9 V, it demonstrates excellent cycle stability and fast-charging capability, substantially outperforming C-LNMO (Fig. 7b,c). After 500 cycles, U-LNMO retains 78.9% of its capacity and continues to deliver over 70 mAh/g at 15 C.

Direct upcycling of spent $LiMn_2O_4$ into Li-rich Mn-based cathode material $Li_{1.2}Ni_{0.2}Mn_{0.6}O_2$

Unlike the phase structure that remains unchanged during the upcycling of LMO to LNMO, the transformation from a spinel structure to a layered structure represents another pathway for achieving direct phase evolution (Fig. 8a). The powders exhibit distinct color changes during this transformation, transitioning from gray–green to reddish-brown. As shown in Fig. 8b, the upcycled Co-free Li-rich Mn-based cathode material (U-LRM) displays the typical structural characteristics. In addition to the main layered structure, a clear superlattice peak of Li_2MnO_3

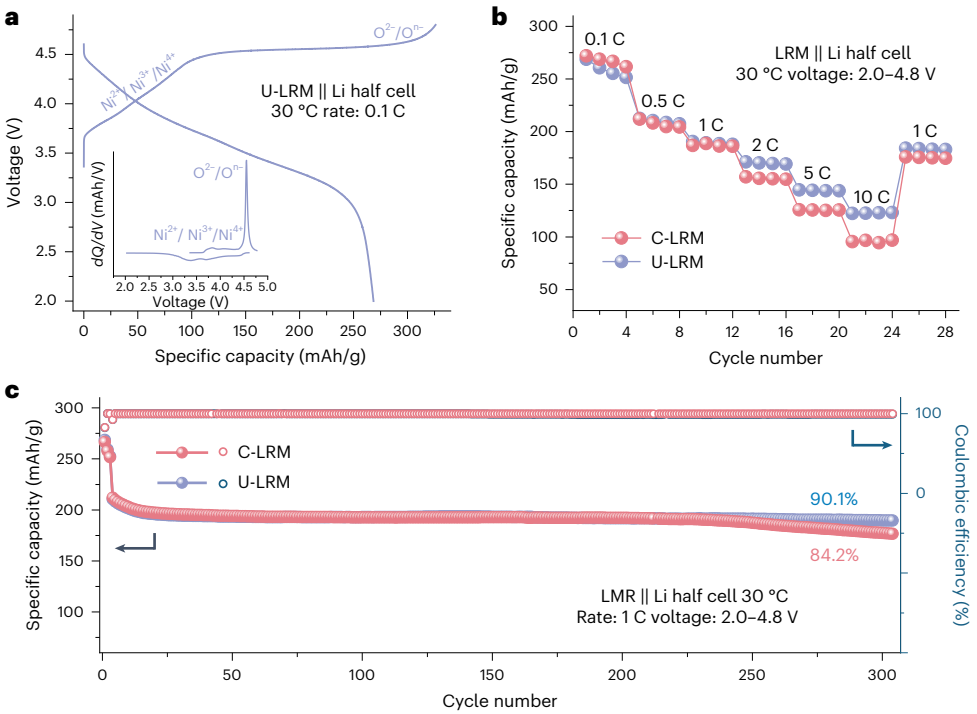

Fig. 9 | Electrochemical performance of upcycled Li-rich Mn-based cathode material $Li_{1.2}Ni_{0.2}Mn_{0.6}O_2$. a, Galvanostatic charge–discharge curve of U-LRM in the voltage range of 2.0–4.8 V at 0.1 C (the inset is the corresponding d*Q*/d*V* curve). **b**, Cycling performance of U-LRM and C-LRM at 1 C. **c**, Rate performance of U-LRM and C-LRM at various current densities.

is observed at ~21°, and the related structural parameters closely match those of the commercial material (C-LRM) (Supplementary Fig. 15 and Supplementary Tables 9 and 10). The phase transition also alters the material's growth planes, resulting in a morphology that deviates from the octahedral structure, forming single crystals with alternative shapes (Fig. 8d). Similar to U-LNMO, U-LRM exhibits two distinct features influenced by the ultrafast nonequilibrium process: the presence of oxygen vacancy defects and a gradient distribution of Ni elements (Fig. 8c,e). Additionally, HRTEM analysis reveals a layered bulk phase with a spinel surface layer, a characteristic effect of oxygen vacancies[64] (Fig. 8f). Electrochemical performance tests indicate that U-LRM exhibits a typical anion redox platform, achieving an impressive first-cycle capacity of 268 mAh/g (Fig. 9a). Its cycle stability and rate performance are slightly superior to those of C-LRM (Fig. 9b,c). After 300 cycles, U-LRM retains 90.1% of its capacity and delivers 122.2 mAh/g at a high current density of 10 C.

Reporting summary

Further information on research design is available in the Nature Portfolio Reporting Summary linked to this article.

Data availability

All of the data supporting this research are available in the main text and the Supplementary Information, and original data can be obtained from the corresponding authors upon reasonable request. Source data are provided with this paper. Other data supporting the findings of this study were previously published[28,35,46,48]. Source data are provided with this paper.

Received: 26 January 2025; Accepted: 12 June 2025;
Published online: 18 August 2025

References

1. Fuso Nerini, F. et al. Mapping synergies and trade-offs between energy and the Sustainable Development Goals. *Nat. Energy* **3**, 10–15 (2018).
2. Soergel, B. et al. A sustainable development pathway for climate action within the UN 2030 agenda. *Nat. Clim. Change* **11**, 656–664 (2021).
3. Li, M., Lu, J., Chen, Z. & Amine, K. 30 years of lithium-ion batteries. *Adv. Mater.* **30**, 1800561 (2018).
4. Yang, X., Liu, T. & Wang, C. Thermally modulated lithium iron phosphate batteries for mass-market electric vehicles. *Nat. Energy* **6**, 176–185 (2021).
5. Huang, Y. & Li, J. Key challenges for grid-scale lithium-ion battery energy storage. *Adv. Energy Mater.* **12**, 2202197 (2022).
6. Lu, D. et al. Ligand-channel-enabled ultrafast Li-ion conduction. *Nature* **627**, 101–107 (2024).
7. Ji, H., Wang, J., Ma, J., Cheng, H.-M. & Zhou, G. Fundamentals, status and challenges of direct recycling technologies for lithium ion batteries. *Chem. Soc. Rev.* **52**, 8194–8244 (2023).
8. Wang, J. et al. Toward direct regeneration of spent lithium-ion batteries: a next-generation recycling method. *Chem. Rev.* **124**, 2839–2887 (2024).
9. Wang, G. et al. Advances and challenges in thermal runaway modelling of lithium-ion batteries. *Innovation* **5**, 100624 (2024).
10. Wang, Z., Zhang, B. & Guan, D. Take responsibility for electronic-waste disposal. *Nature* **536**, 23–25 (2016).
11. Bauer, C. et al. Charging sustainable batteries. *Nat. Sustain.* **5**, 176–178 (2022).
12. Gent, W. E., Busse, G. M. & House, K. Z. The predicted persistence of cobalt in lithium-ion batteries. *Nat. Energy* **7**, 1132–1143 (2022).
13. Sun, X., Ouyang, M. & Hao, H. Surging lithium price will not impede the electric vehicle boom. *Joule* **6**, 1738–1742 (2022).
14. Harper, G. et al. Recycling lithium-ion batteries from electric vehicles. *Nature* **575**, 75–86 (2019).
15. Harper, G. D. J. Upcycle for enhanced performance. *Nat. Sustain.* **6**, 725–726 (2023).
16. Chen, W. et al. Recycling lithium-ion batteries from electric vehicles. *Sci. Adv.* **9**, eadh5131 (2023).
17. Tran, M. K., Rodrigues, M.-T. F., Kato, K., Babu, G. & Ajayan, P. M. Deep eutectic solvents for cathode recycling of Li-ion batteries. *Nat. Energy* **4**, 339–345 (2019).
18. Cao, Y. et al. A review of direct recycling methods for spent lithium-ion batteries. *Energy Storage Mater.* **70**, 103475 (2024).
19. Tao, Y., Rahn, C. D., Archer, L. A. & You, F. Second life and recycling: energy and environmental sustainability perspectives for high-performance lithium-ion batteries. *Sci. Adv.* **7**, eabi7633 (2021).
20. Ciez, R. E. & Whitacre, J. F. Examining different recycling processes for lithium-ion batteries. *Nat. Sustain.* **2**, 148–156 (2019).
21. Lan, Y. et al. Direct regenerating cathode materials from spent lithium-ion batteries. *Adv. Sci.* **11**, 2304425 (2024).
22. Frith, J. T., Lacey, M. J. & Ulissi, U. A non-academic perspective on the future of lithium-based batteries. *Nat. Commun.* **14**, 420 (2023).
23. Ren, H. et al. Densification of cathode/electrolyte interphase to enhance reversibility of $LiCoO_2$ at 4.65 V. *Adv. Mater.* **36**, 2408875 (2024).
24. Xue, H. et al. In situ conversion of artificial proton-rich shell to inorganic maskant toward stable single-crystal Ni-rich cathode. *Adv. Mater.* **37**, 2415860 (2025).
25. Xu, E. et al. Stress-induced anomalous lithiation plateau of $LiFe_yMn_{1-y}PO_4$ over high-rate discharging. *Adv. Energy Mater.* **15**, 2404929 (2025).
26. Zhu, X. et al. Epitaxial growth of an atom-thin layer on a $LiNi_{0.5}Mn_{1.5}O_4$ cathode for stable Li-ion battery cycling. *Nat. Commun.* **13**, 1565 (2022).
27. Liu, T. et al. Origin of structural degradation in Li-rich layered oxide cathode. *Nature* **606**, 305–312 (2022).
28. Wang, J. et al. Sustainable upcycling of spent $LiCoO_2$ to an ultra-stable battery cathode at high voltage. *Nat. Sustain.* **6**, 797–805 (2023).
29. Zheng, N. et al. Surface catalytic repair for the efficient regeneration of spent layered oxide cathodes. *J. Am. Chem. Soc.* **146**, 27819–27829 (2024).
30. Ji, G. et al. Direct regeneration of degraded lithium-ion battery cathodes with a multifunctional organic lithium salt. *Nat. Commun.* **14**, 584 (2023).
31. Tang, D. et al. A multifunctional amino acid enables direct recycling of spent $LiFePO_4$ cathode material. *Adv. Mater.* **36**, 2309722 (2024).
32. Jia, K. et al. Topotactic transformation of surface structure enabling direct regeneration of spent lithium-ion battery cathodes. *J. Am. Chem. Soc.* **145**, 7288–7300 (2023).
33. Wang, J. et al. Direct and green repairing of degraded $LiCoO_2$ for reuse in lithium-ion batteries. *Natl Sci. Rev.* **9**, nwac097 (2022).
34. Ma, J. et al. Adaptable eutectic salt for the direct recycling of highly degraded layer cathodes. *J. Am. Chem. Soc.* **144**, 20306–20314 (2022).
35. Wang, J. et al. Direct recycling of spent cathode material at ambient conditions via spontaneous lithiation. *Nat. Sustain.* **7**, 1283–1293 (2024).
36. Shi, R. et al. Homogeneous repair of highly degraded Ni-rich cathode material with spent lithium anode. *Adv. Mater.* **36**, 2311553 (2024).
37. Zhuang, Z. et al. Fast Li replenishment channels-assisted recycling of degraded layered cathodes with enhanced cycling performance and thermal stability. *Adv. Mater.* **36**, 2313144 (2024).
38. Li, J. et al. Interfacial metal-solvent chelation for direct regeneration of $LiFePO_4$ cathode black mass. *Adv. Mater.* **37**, 2414235 (2025).
39. Chen, W. et al. Efficient and scalable direct regeneration of spent layered cathode materials via advanced oxidation. *Adv. Mater.* **37**, 2414235 (2025).
40. Choi, C. H. et al. Flash-within-flash synthesis of gram-scale solid-state materials. *Nat. Chem.* **16**, 1831–1837 (2024).
41. Wang, C. et al. A general method to synthesize and sinter bulk ceramics in seconds. *Science* **369**, 521–526 (2020).
42. Zhu, W. et al. Ultrafast non-equilibrium synthesis of cathode materials for Li-ion batterie. *Adv. Mater.* **35**, 2208974 (2023).
43. Guo, Z. et al. Ultrafast non-equilibrium phase transition induced twin boundaries of spinel lithium manganate. *Adv. Energy Mater.* **14**, 2302484 (2024).
44. Guo, Y. et al. Atomistic observation and transient reordering of antisite Li/Fe defects toward sustainable $LiFePO_4$. *Energy Environ. Sci.* **17**, 7749–7761 (2024).
45. Yin, Y. et al. Rapid, direct regeneration of spent $LiCoO_2$ cathodes for Li-ion batteries. *ACS Energy Lett.* **8**, 3005–3012 (2023).
46. Ji, H. et al. Closed-loop direct upcycling of spent Ni-rich layered cathodes into high-voltage cathode materials. *Adv. Mater.* **36**, 2407029 (2024).
47. Ji, G. et al. Sustainable upcycling of mixed spent cathodes to a high-voltage polyanionic cathode material. *Nat. Commun.* **15**, 4086 (2024).
48. Ma, J. et al. Subtractive transformation of cathode materials in spent Li-ion batteries to a low-cobalt 5 V-class cathode material. *Nat. Commun.* **15**, 1046 (2024).
49. Liu, S. et al. Manganese-based composite-structure cathode materials for sustainable batteries. *Adv. Energy Mater.* **15**, 2404459 (2025).
50. Song, J. et al. Building better full manganese-based cathode materials for next-generation lithium-ion batteries. *Electrochem. Energy Rev.* **6**, 20 (2023).
51. Gupta, V. et al. Scalable direct recycling of cathode black mass from spent lithium-ion batteries. *Adv. Energy Mater.* **13**, 2203093 (2023).
52. Tao, S. et al. Collaborative and privacy-preserving retired battery sorting for profitable direct recycling via federated machine learning. *Nat. Commun.* **14**, 8032 (2023).
53. Tao, S. et al. Generative learning assisted state-of-health estimation for sustainable battery recycling with random retirement conditions. *Nat. Commun.* **15**, 10154 (2024).
54. Chen, Z. et al. Reaction-passivation mechanism driven materials separation for recycling of spent lithium-ion batteries. *Nat. Commun.* **14**, 4649 (2023).
55. Ji, H. et al. Surface engineering suppresses the failure of biphasic sodium layered cathode for high performance sodium-ion batteries. *Adv. Funct. Mater.* **32**, 2109319 (2022).
56. Zhang, Y. et al. Operando characterization and regulation of metal dissolution and redeposition dynamics near battery electrode surface. *Nat. Nanotechnol.* **19**, 790–797 (2023).
57. Zeng, W. et al. Entropy-increased $LiMn_2O_4$-based positive electrodes for fast-charging lithium metal batteries. *Nat. Commun.* **15**, 7371 (2024).
58. Liu, T. et al. Correlation between manganese dissolution and dynamic phase stability in spinel-based lithium-ion battery. *Nat. Commun.* **10**, 4721 (2019).
59. Tan, Y. et al. Overlithiation-driven structural regulation of lithium nickel manganese oxide for high-performance battery cathode. *Energy Storage Mater.* **63**, 102962 (2023).
60. Dong, Q., Hu, S. & Hu, L. Electrothermal synthesis of commodity chemicals. *Nat. Chem. Eng.* **1**, 680–690 (2024).
61. Wang, R. et al. Twin boundary defect engineering improves lithium-ion diffusion for fast-charging spinel cathode materials. *Nat. Commun.* **12**, 3085 (2021).
62. Zhang, Y. et al. Oxygen vacancy chemistry in oxide cathodes. *Chem. Soc. Rev.* **53**, 3302–3326 (2024).
63. Zhang, X. et al. Surface nickel gradient tunes anionic redox activity to stabilize cobalt-free Li-rich cathodes. *Nano Energy* **128**, 109973 (2024).
64. Wang, K. et al. Unraveling the role of surficial oxygen vacancies in stabilizing Li-rich layered oxides. *Adv. Energy Mater.* **13**, 2301216 (2023).

Acknowledgements

G.Z. was supported by the Guangdong Innovative and Entrepreneurial Research Team Program (grant no. 2021ZT09L197), Shenzhen Science and Technology Program (grant no. KQTD20210811090112002), the Interdisciplinary Research and Innovation Fund of Tsinghua Shenzhen International Graduate School and the Tsinghua Shenzhen International Graduate School-Shenzhen Pengrui Young Faculty Program of Shenzhen Pengrui Foundation (grant no. SZPR2023007). H.J. was supported by the National Natural Science Foundation of China (grant no. 524B2023). J.W. was supported by the Startup Fund for Young Faculty at Shanghai Jaio Tong University (grant no. 23×010502206) and the National Natural Science Youth Fund (grant no. 52302285).

Author contributions

H.J., J.W., G.Z. and H.-M.C. conceived the idea and provided design guidelines. H.J. and J.W. performed the relevant experiments and data analysis with the help of X.Q., H.R., H.X., H.Z. and G.J. All authors discussed and contributed to the results. H.J. wrote the manuscript with comments and revisions from all the authors.

Competing interests

The authors declare no competing interests.

Additional information

Supplementary information The online version contains supplementary material available at https://doi.org/10.1038/s41596-025-01234-9.

Correspondence and requests for materials should be addressed to Hui-Ming Cheng or Guangmin Zhou.

Peer review information *Nature Protocols* thanks Hao Luo and Min-Sik Park for their contribution to the peer review of this work.

[1]Tsinghua Shenzhen International Graduate School, Tsinghua University, Shenzhen, China. [2]Frontiers Science Center for Transformative Molecules, School of Chemistry and Chemical Engineering, Shanghai Jiao Tong University, Shanghai, China. [3]Department of Electronic and Computer Engineering, The Hong Kong University of Science and Technology, Kowloon, Hong Kong SAR, China. [4]School of Advanced Materials, Peking University Shenzhen Graduate School, Shenzhen, China. [5]Faculty of Materials Science and Energy Engineering and Institute of Technology for Carbon Neutrality, Shenzhen Institute of Advanced Technology, Chinese Academy of Sciences, Shenzhen, China. [6]Shenyang National Laboratory for Materials Science, Institute of Metal Research, Chinese Academy of Sciences, Shenyang, China. [7]These authors contributed equally: Haocheng Ji, Junxiong Wang.

nature portfolio

Corresponding author(s): Hui-Ming Cheng and Guangmin Zhou

Last updated by author(s): May 13, 2025

Reporting Summary

Nature Portfolio wishes to improve the reproducibility of the work that we publish. This form provides structure for consistency and transparency in reporting. For further information on Nature Portfolio policies, see our Editorial Policies and the Editorial Policy Checklist.

Statistics

For all statistical analyses, confirm that the following items are present in the figure legend, table legend, main text, or Methods section.

n/a	Confirmed	
☐	☒	The exact sample size (*n*) for each experimental group/condition, given as a discrete number and unit of measurement
☒	☐	A statement on whether measurements were taken from distinct samples or whether the same sample was measured repeatedly
☒	☐	The statistical test(s) used AND whether they are one- or two-sided *Only common tests should be described solely by name; describe more complex techniques in the Methods section.*
☒	☐	A description of all covariates tested
☒	☐	A description of any assumptions or corrections, such as tests of normality and adjustment for multiple comparisons
☐	☒	A full description of the statistical parameters including central tendency (e.g. means) or other basic estimates (e.g. regression coefficient) AND variation (e.g. standard deviation) or associated estimates of uncertainty (e.g. confidence intervals)
☒	☐	For null hypothesis testing, the test statistic (e.g. *F*, *t*, *r*) with confidence intervals, effect sizes, degrees of freedom and *P* value noted *Give P values as exact values whenever suitable.*
☒	☐	For Bayesian analysis, information on the choice of priors and Markov chain Monte Carlo settings
☒	☐	For hierarchical and complex designs, identification of the appropriate level for tests and full reporting of outcomes
☒	☐	Estimates of effect sizes (e.g. Cohen's *d*, Pearson's *r*), indicating how they were calculated

Our web collection on statistics for biologists contains articles on many of the points above.

Software and code

Policy information about availability of computer code

Data collection	None
Data analysis	EverBatt2023 (https://www.anl.gov/amd/everbatt) OriginPro (https://www.originlab.com) MDI Jade (https://www.icdd.com/mdi-jade) FullProf (https://www.ill.eu/sites/fullprof/php/downloads.html) Digital Micrograp (https://www.gatan.com/products/tem-analysis/gatan-microscopy-suite-software) NEWARE BTS9.0 (https://www.neware.com.cn/)

For manuscripts utilizing custom algorithms or software that are central to the research but not yet described in published literature, software must be made available to editors and reviewers. We strongly encourage code deposition in a community repository (e.g. GitHub). See the Nature Portfolio guidelines for submitting code & software for further information.

Data

Policy information about availability of data

All manuscripts must include a data availability statement. This statement should provide the following information, where applicable:

- Accession codes, unique identifiers, or web links for publicly available datasets
- A description of any restrictions on data availability
- For clinical datasets or third party data, please ensure that the statement adheres to our policy

All of the data supporting this research are available in the main text and the Supplementary Information, and original data can be obtained from the corresponding authors upon reasonable request. Source data are provided with this paper. And other data supporting the findings of this study were previously published [28, 35, 46, 48].

Research involving human participants, their data, or biological material

Policy information about studies with human participants or human data. See also policy information about sex, gender (identity/presentation), and sexual orientation and race, ethnicity and racism.

Reporting on sex and gender	None
Reporting on race, ethnicity, or other socially relevant groupings	None
Population characteristics	None
Recruitment	None
Ethics oversight	None

Note that full information on the approval of the study protocol must also be provided in the manuscript.

Field-specific reporting

Please select the one below that is the best fit for your research. If you are not sure, read the appropriate sections before making your selection.

☐ Life sciences ☐ Behavioural & social sciences ☒ Ecological, evolutionary & environmental sciences

For a reference copy of the document with all sections, see nature.com/documents/nr-reporting-summary-flat.pdf

Ecological, evolutionary & environmental sciences study design

All studies must disclose on these points even when the disclosure is negative.

Study description	This protocol presents a general strategy for the direct regeneration of spent lithium-ion battery cathode materials to restore their original performance or upcycle them into next-generation cathodes with enhanced capabilities.
Research sample	Spent LIBs Cathode materials
Sampling strategy	Each testing group contains at least three parallel samples to ensure the reliability and repeatability of the test battery performance.
Data collection	All battery test data are automatically recorded by the battery test system.
Timing and spatial scale	The start and end of the battery test are based on the voltage. The charge and discharge test will start when the voltage reaches theset value of charge and discharge cut-off voltage, respectively. The whole cycle test will end when the battery capacity decays to acertain extent.
Data exclusions	No data was excluded.
Reproducibility	Each group of test cells has at least three parallel samples to ensure reproducibility of experimental results.
Randomization	This is not relevant to this study. The selection of experimental samples and test conditions are strictly controlled and kept consistent, so there is no randomization in this study.
Blinding	This is not relevant to this study. There are many researches on recycling of cathode materials, and there are many referable results,which are very clear. The results of this paper are clear, and all the details are described carefully, so there is no problem of blinding.

Did the study involve field work? ☐ Yes ☒ No

Reporting for specific materials, systems and methods

We require information from authors about some types of materials, experimental systems and methods used in many studies. Here, indicate whether each material, system or method listed is relevant to your study. If you are not sure if a list item applies to your research, read the appropriate section before selecting a response.

Materials & experimental systems

n/a	Involved in the study
☒	☐ Antibodies
☒	☐ Eukaryotic cell lines
☒	☐ Palaeontology and archaeology
☒	☐ Animals and other organisms
☒	☐ Clinical data
☒	☐ Dual use research of concern
☒	☐ Plants

Methods

n/a	Involved in the study
☒	☐ ChIP-seq
☒	☐ Flow cytometry
☒	☐ MRI-based neuroimaging